Nuclear Physics **A413** (1984) 375–415

INTRINSIC REFLECTION ASYMMETRY IN ODD-*A* NUCLEI

G.A. LEANDER

UNISOR, Oak Ridge Associated Universities, Oak Ridge, Tennessee, USA[†]
and
Department of Chemistry, Florida State University, Tallahassee, Florida, USA

and

R.K. SHELINE

Department of Chemistry, Florida State University, Tallahassee, Florida, USA

Received 16 August 1983

Abstract: A theoretical description is formulated for odd-A nuclei whose intrinsic shape is axially elongated and statically or dynamically reflection asymmetric. It is used to evaluate data in the Ra-Ac-Th-Pa region on energy levels, decoupling factors, α-transitions and electromagnetic M1, E1 and E3 matrix elements. The results provide firm empirical evidence for a predicted transition from octupole vibrations above $A \sim 229$ to more or less stable octupole deformation in lighter isotopes. Some parity-mixed Nilsson orbitals resulting from strong coupling to the intrinsic reflection asymmetry can be identified.

1. Introduction

1.1. HISTORICAL BACKGROUND

The "quasimolecular" nuclear model introduced by Bohr [1]) in 1952 states that a piece of nuclear matter may acquire an asymmetric shape in its intrinsic frame of reference, and just as with molecules the properties of the individual nuclear species is intimately connected with the shape and its symmetries. In nuclei, reflection *symmetric* shapes of spheroidal ($D_{\infty h}$) or ellipsoidal (D_{2h}) symmetry have mainly been considered. Intrinsic reflection *asymmetry* would be fundamentally interesting since new physical situations and insights can be expected from the additional symmetry breaking. It is well known from molecular spectroscopy that a signature of reflection asymmetry is the splitting of each quantal state into two near-degenerate states of opposite parity [e.g. ref. [2])], and the possibility of such shapes was considered [3]) after low-lying negative-parity states had been discovered [4]) in doubly even nuclei of the radium region. Axial $C_{\infty h}$ symmetry was suggested by the observation that γ-transition intensities from these negative-parity states into the positive-parity levels follow the rule

$$B(\mathrm{E1}; I_i\pi = - \rightarrow I_f\pi = +) \propto |\langle I_i K 10 | I_f K \rangle|^2 \qquad (1.1)$$

[†] Permanent address.

with K in the Clebsch–Gordan coefficient equal to zero. However, a consensus was formed after many theoretical investigations that well-developed reflection asymmetric shapes do not occur in nuclei. Whereas the energy splitting of the parity doublets in molecules is small compared to the overall energy scale of the excitation spectrum, the parity splitting in nuclei is typically larger than the energy associated with rotations and, in odd nuclei, the quasiparticle degree of freedom. The negative-parity states of doubly even radium and thorium nuclei were described as coherent but non-adiabatic vibrations built from few-quasiparticle excitations in the reflection symmetric representation [5]. Opposite-parity states in odd-A nuclei have been attributed to unrelated Nilsson orbitals of good parity [6].

In recent years, new experimental and theoretical evidence [e.g. refs. [7-13])] has revived the concept of intrinsic reflection asymmetry in the radium region†. The present work extends the investigation of ref. [10]), where further references to the earlier literature can be found. This previous paper [10]) presented potential-energy-of-deformation surfaces from macroscopic–microscopic calculations, with minima at finite octupole (reflection asymmetric) as well as quadrupole axial deformation. The consequences of octupole deformation were found to be consistent with experimental mass measurements and, less conclusively, the spectroscopy of even and odd-mass nuclei. The purpose of the present paper is:

(i) To update the theory of quasiparticle coupling to a core with static or dynamical $C_{\infty h}$ symmetry (sect. 2). A guide to optimally simple but accurate models is obtained by pursuing analogies with standard ways of handling $D_{\infty h}$ symmetry. The basic philosophy is explained in subsect. 1.2.

(ii) Thereafter, in sects. 3 and 4, to investigate the validity and spectroscopic implications of the previous results [10]) with the help of these models; in particular, to see whether experimental data in odd-A nuclei of the Ra region provide positive evidence for octupole deformation by manifesting parity-mixed Nilsson orbitals.

1.2. ANALOGY BETWEEN PARITY DOUBLETS AND ROTATIONAL BANDS

A proven method of nuclear structure theory is to start out in a postulated intrinsic frame of reference, where symmetries may break spontaneously even though they are symmetries of the full hamiltonian and give rise to good quantum numbers in the laboratory frame. Fig. 1 illustrates the familiar procedure with respect to spherical symmetry and analogously with respect to reflection symmetry.

The ground-state spin of a doubly even nucleus is zero, which is equivalent to spherical symmetry. For most nuclei, however, the mean-field approximation describes the equilibrium configuration as elongated in some "arbitrary" direction which thereby defines a principal axis of the intrinsic frame. Spherical symmetry is broken and the intrinsic equilibrium configuration is a superposition of many spins.

† We have been informed that the results of ref. [9]) are due to an error by a factor of 2 in the computer code.

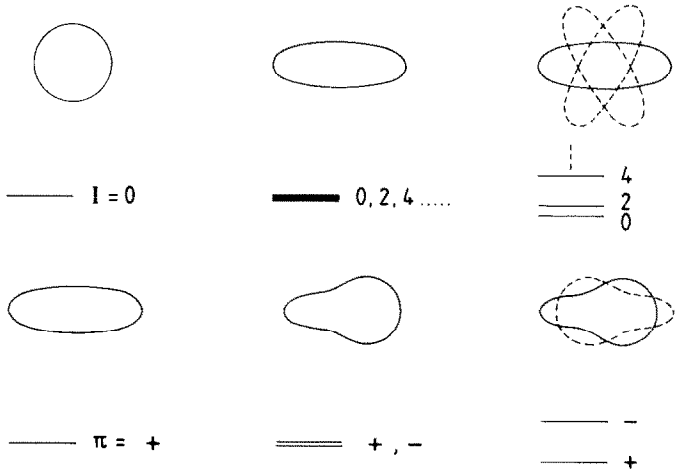

Fig. 1. Spontaneous symmetry breaking in doubly even nuclei is represented schematically for rotational symmetry (above) and reflection symmetry (below). The figures in the middle are in the intrinsic frame of reference, while those to the right have been projected back into the laboratory frame.

The spherical symmetry can be restored by projection, which gives a wave function with equal probability for all orientations of the intrinsic frame. It is also possible to project out the other spins. In general the different spin states are not degenerate with respect to the full hamiltonian, but they are nevertheless revealed as manifestations of a single intrinsic configuration by fast in-band collective E2 transitions. An odd-mass nucleus has an additional particle in a Nilsson orbital in the intrinsic frame. This one intrinsic orbital is manifested in each of the spin states by its intrinsic matrix elements, for example the magnetic moment.

The technique outlined above provides the basis for many nuclear structure studies, and in some regions of nuclei it is fairly accurate *per se* [2]). The single-particle orbitals associated with spheroidal intrinsic symmetry [14]) have largely been identified in experiment [6]). The present investigation shows how Nilsson orbitals associated with intrinsic reflection asymmetry might be recognized, and evaluates the information presently available from experiment in the actinium ($Z = 89$) region. The analog of a rotational band for reflection asymmetry is a parity doublet (fig. 1), connected by E1 and E3 transitions which reflect the intrinsic dipole and octupole moments. The criterion to be used in identifying such a doublet is not so much the smallness of the energy splitting, which can be misleading, but rather the similarity of the intrinsic configurations. In odd-mass nuclei the two members of a doublet should correspond to a single parity-mixed intrinsic orbital.

2. Theory

Two alternative spectroscopic models will be formulated and studied. Both describe a quasiparticle coupled to a rotor core which has an intrinsic $K = 0$ reflection

asymmetric degree of freedom. One is a model of strong coupling between the particle and the reflection asymmetric intrinsic field. Then the basis states themselves contain parity-mixed Nilsson states. The other is a model of intermediate coupling to reflection asymmetry and is based on the conventional Nilsson orbitals of good parity. Depending on which scheme achieves the best description of experimental data, or which basis is most nearly diagonal, one may try to judge whether reflection asymmetric or symmetric Nilsson orbitals are the most appropriate to characterize the physical states.

The strong and intermediate coupling formalisms described in subsects. 2.2 and 2.3, respectively, have evolved from many predecessors. In particular, strong coupling was considered by Krappe and Wille [15]) while Faessler *et al.* [16]) made an early study of odd-particle coupling to a $K^{\pi}=0^{-}$ octupole phonon. The intrinsic single-particle hamiltonian employed is described in subsect. 2.1. There we shall also become acquainted with nuclides that are proposed to be reflection asymmetric, and with the particular Nilsson orbitals that might be observed in these nuclei – both the reflection asymmetric ones and the symmetric orbitals previously used for labelling [6]).

2.1. INTRINSIC SINGLE-PARTICLE STATES

Adiabatic single-particle motion in the intrinsic frame of the nuclear mean field is described by the deformed shell model. The Schrödinger equation is solved for independent fermions in a potential well which can have quadrupole, octupole and other multipole distortions from spherical symmetry. Nilsson's modified oscillator potential [14]) is adequate and convenient for most purposes. However, the coupling to octupole deformation is stronger in a potential with a more realistic flat-bottomed radial shape [10]), reflecting the fact that octupole shell structure does not occur in an oscillator potential [2]). Therefore a folded Yukawa single-particle potential is employed in the present work. Studies by other researchers using a Woods–Saxon potential [17,18]) or simply a renormalization of the oscillator octupole coordinate ε_3 to larger values [9]) are presumably compatible.

The folded Yukawa potential was proposed by the Los Alamos group [19]) in 1972, a set of parameters was fitted [20]) to the Nilsson levels of actinide nuclei in 1974, and instability with respect to octupole deformation for nuclei around ^{222}Ra was noted for the first time in any single-particle potential [8]) in 1981. The octupole-deformed minima in the potential energy of deformation were calculated for this whole region of nuclei in a subsequent investigation [10]). It turns out that the lowering of the ground-state energy due to the octupole degree of freedom systematically improves the agreement with experimental masses. The single-particle energies and wave functions, ground-state shapes and potential-energy curves employed in the present work are based on the methods and results from this previous work. In practice, single-particle wave functions have been calculated with the hexadecapole

TABLE 1

The function $\varepsilon_4(\varepsilon_2, \varepsilon_3)$ employed in the present work

ε_2	$\varepsilon_3 = 0.00$	0.04	0.08	0.12
0.09	−0.050	−0.050	−0.050	−0.045
0.10	−0.060	−0.060	−0.060	−0.055
0.11	−0.065	−0.065	−0.065	−0.060
0.12	−0.070	−0.070	−0.065	−0.060
0.13	−0.070	−0.070	−0.065	−0.060
0.14	−0.070	−0.070	−0.065	−0.060
0.15	−0.080	−0.075	−0.068	−0.060
0.16	−0.085	−0.080	−0.070	−0.060
0.17	−0.080	−0.075	−0.068	−0.060
0.18	−0.075	−0.070	−0.063	−0.055
0.19	−0.075	−0.070	−0.063	−0.055

This table supplements ref. [10]) in specifying details of the calculations.

coordinate ε_4 as a single-valued function of ε and ε_3, determined at each point by minimization of the potential energy for the most relevant radium or thorium isotope. For completeness and future reference, this function is specified in table 1.

The folded Yukawa single-particle levels are plotted in figs. 2–5 as a function of the quadrupole deformation ε, for $\varepsilon_3 = 0$ and 0.08. The nuclei in the region of ground-state octupole deformation, $85 \lesssim Z \lesssim 92$ and $131 \lesssim N \lesssim 139$, have ε deformations which increase smoothly over the abscissa in figs. 2–5 with increasing neutron and proton number. The calculated ε_3 deformation in most of this region is $\varepsilon_3 = 0.08$–0.10.

Each level for $\varepsilon_3 = 0$ in figs. 2 and 3 is labelled by the usual [20]) large component in Nilsson's asymptotic representation $[Nn_z\Lambda]\Omega$. The detailed structure of the reflection symmetric levels has been described extensively in the literature [e.g. refs. [21,22])]. The asymmetric levels for $\varepsilon_3 = 0.08$ in figs. 4 and 5 are labelled by the good quantum number Ω, which is the total angular momentum component along the symmetry axis. In general, the reflection asymmetric Nilsson orbitals are strongly parity-mixed. Typically they might contain about equal admixtures of two symmetric orbitals which lie close in energy for $\varepsilon_3 = 0$ and have the same Ω but opposite parities $\pi = (-)^N$. For example, $[642]\frac{5}{2}$ and $[523]\frac{5}{2}$, located just above the $Z = 92$ gap at $\varepsilon_3 = 0$ (fig. 3), are the largest components in the $\Omega = \frac{5}{2}$ proton orbital occupied by the 91st proton at $\varepsilon_3 = 0.08$ (fig. 5). The latter parity-mixed Nilsson orbital may be responsible for a $\frac{5}{2}^{\pm}$ ground-state doublet that was recently observed [12]) in $^{229}_{91}$Pa.

Explicit formulas are available in the literature [23]) for matrix elements of the single-particle angular momentum operators, in the basis and with the phase conventions of the folded Yukawa model [19]). In figs. 4 and 5 the expectation values of some single-particle operators are indicated in parentheses. The first, $\langle \hat{s}_z \rangle$, can be used in conjunction with Ω to calculate magnetic moments [14]). The second, $\langle \hat{\pi} \rangle$,

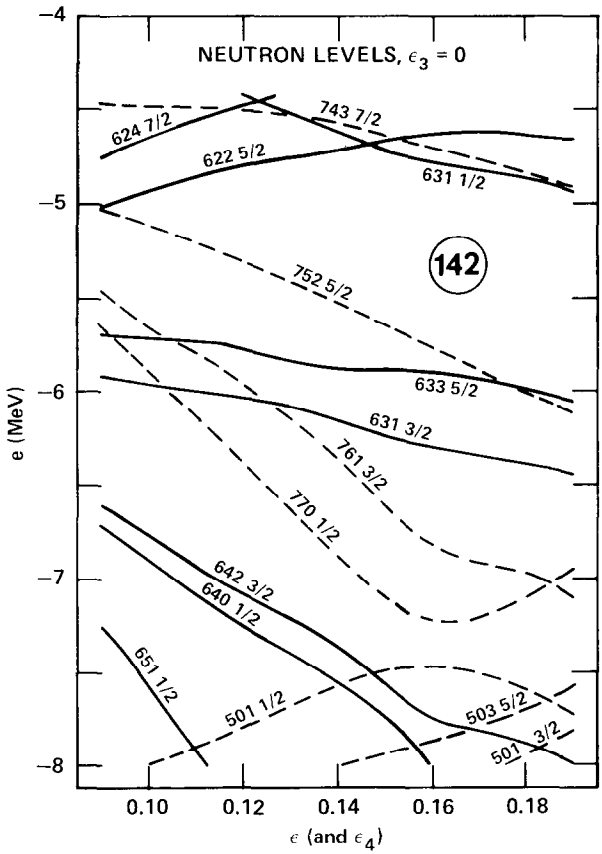

Fig. 2. Single-neutron orbitals in a folded Yukawa potential with spheroidal symmetry ($\varepsilon_3 = 0$), plotted versus the elongation coordinate ε. They are labelled by the same large component $Nn_z\Lambda\Omega$ as in ref. [20]). Positive- and negative-parity orbitals are represented by solid and dashed curves, respectively.

may vary from -1 to $+1$ and equals zero for an equal admixture of positive- and negative-parity components. The additional number for $\Omega = \frac{1}{2}$ is an expectation value of $\hat{j}_+$ between conjugate states defined in subsect. 2.2, with a physical interpretation as the parity times the decoupling parameter. None of the expectation values change very much as a function of ε, staying within ± 0.1 units of the indicated values over the entire range of figs. 4 or 5. However, they are often quite sensitive to variations in ε_3. A plot of single-neutron levels in ref. [10]) illustrates the complicated pattern of strong interactions between orbitals as a function of ε_3.

2.2. STRONG COUPLING

The strong-coupling scheme assumes that the hamiltonian can be written in two parts describing the rotational motion of the intrinsic frame and the intrinsic degrees

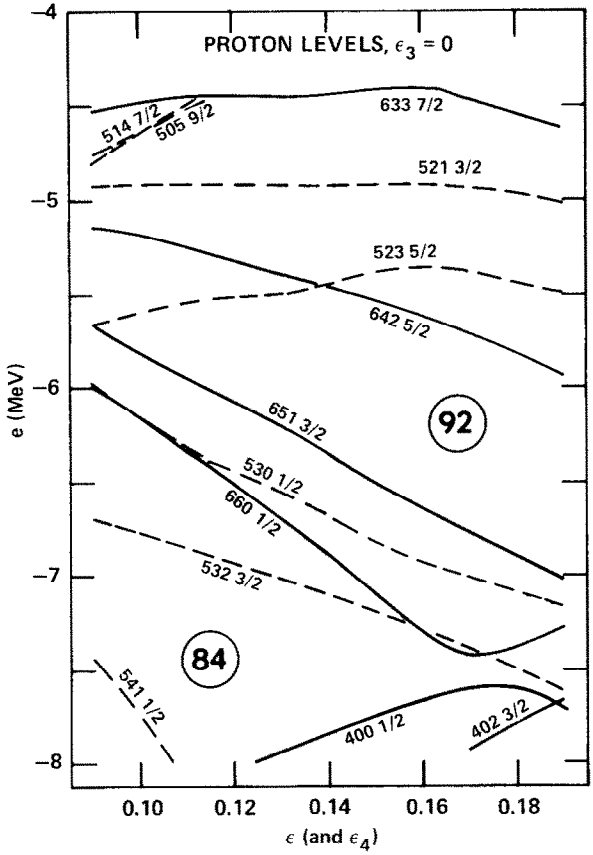

Fig. 3. Same as fig. 1 but for protons.

of freedom

$$\hat{H} = \hat{H}_{\text{rotor}} + \hat{H}_{\text{intr}} . \tag{2.1}$$

The rotor part is characterized by at least one moment of inertia parameter which could be computed microscopically, though for the purpose of a core-particle coupling calculation it is better to take an empirical value from the neighboring doubly even nuclei. With axial symmetry [2])

$$\hat{H}_{\text{rotor}} = \frac{\hbar^2}{2\mathcal{I}} \hat{\boldsymbol{R}}^2 = \frac{\hbar^2}{2\mathcal{I}} (\hat{\boldsymbol{I}} - \hat{\boldsymbol{j}})^2 . \tag{2.2}$$

The intrinsic part of $\hat{H}$ is

$$\hat{H}_{\text{intr}} = \hat{H}_{\text{core}} + [\hat{H}_{\text{s.p.}} + \hat{H}_{\text{pair}}]_{\epsilon_3 = \bar{\epsilon}_3} . \tag{2.3}$$

The deformed single-particle potential in $\hat{H}_{\text{s.p.}}$ is the folded Yukawa potential described above, $\hat{H}_{\text{pair}}$ is the standard BCS pairing in this model, and ε_3 is the

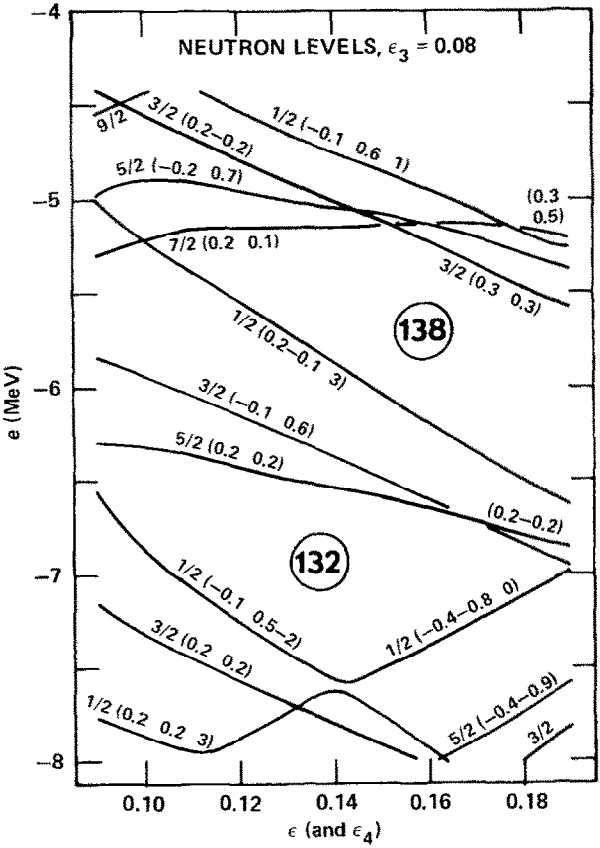

Fig. 4. Single-neutron orbitals in an axially symmetric but reflection asymmetric folded Yukawa potential ($\varepsilon_3 = 0.08$), plotted versus the quadrupole elongation coordinate ε. The orbitals are labelled by Ω and, in parentheses, a set of single-particle matrix elements: $\langle \hat{s}_z \rangle, \langle \hat{\pi} \rangle$ and if $\Omega = \frac{1}{2}$ also $\langle \pi \text{ conj} | -\hat{j}_+ | R \text{ conj} \rangle$.

reflection asymmetry coordinate. The parity splitting in the doubly even core is taken into account in complete analogy with angular momentum splitting in the rotor:

$$\hat{H}_{\text{core}} = \tfrac{1}{2}E(1-\hat{P}) = \tfrac{1}{2}E(1-p\hat{\pi})\,. \tag{2.4}$$

$\hat{P}$ is the core parity operator which can be written as the product of the single-particle parity operator $\hat{\pi}$ and the total parity $p = \pm 1$. The "inertia parameter" E might again be calculated microscopically but is more accurately obtained empirically from the doubly even neighbors. There the core parity $\hat{P}$ is diagonal and E is the observed parity splitting between the ground state and the virtual $K^\pi = 0^-$ band head. The single-particle parity operator $\hat{\pi}$ appears as the analog of the rotational Coriolis operator $\hat{j}_+$ and plays a corresponding role as will be seen below. The 1 in eq. (2.4) is the analog of the rotational recoil term; both of these terms will henceforth be dropped.

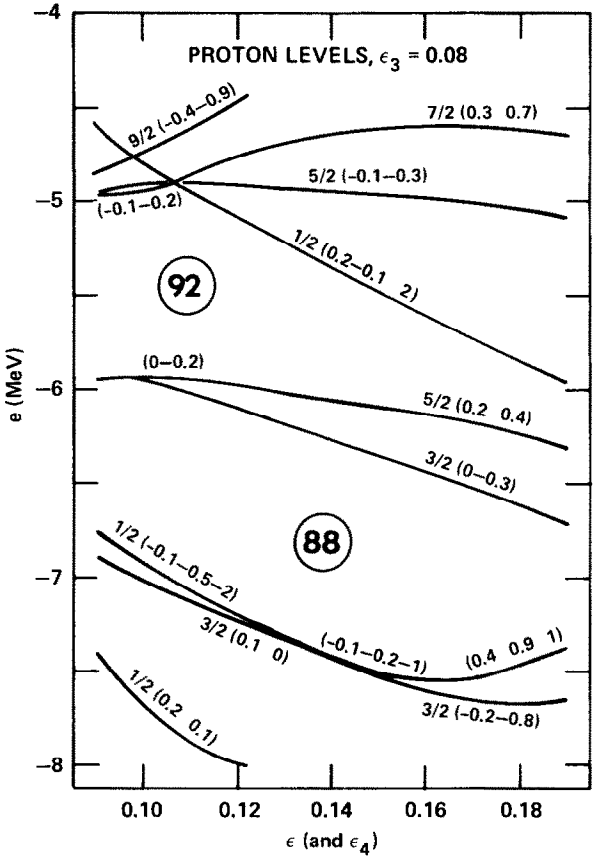

Fig. 5. Same as fig. 3 but for protons.

The solution of the strong-coupling hamiltonian proceeds in the following steps:

(i) $\hat{H}_{\text{s.p.}}$ is diagonalized for $\varepsilon_3 = \bar{\varepsilon}_3$, which gives single-particle energies ε_Ω and wave functions Ψ_Ω.

(ii) $\hat{H}_{\text{pair}}$ is diagonalized in the usual BCS approximation to give quasiparticle energies and wave functions

$$\varepsilon_\Omega \to \tilde{\varepsilon}_\Omega, \qquad \Psi_\Omega \to \tilde{\Psi}_\Omega . \tag{2.5}$$

(iii) The core space is spanned by

$$\Phi_a(\varepsilon_3) = \delta(\varepsilon_3 = \bar{\varepsilon}_3) , \qquad \Phi_b(\varepsilon_3) = \delta(\varepsilon_3 = -\bar{\varepsilon}_3) , \tag{2.6}$$

with the symmetries

$$\hat{P}\Phi_a = \Phi_b , \qquad \hat{R}_1 \Phi_a = \Phi_b . \tag{2.7}$$

$\hat{R}_1$ is the operator which changes y to $-y$, z to $-z$.

(iv) The space of $\hat{H}_{\rm intr}$ is spanned by states of good total parity $p = \pm 1$:

$$\chi^{\rm intr}_{\Omega p} = \sqrt{\tfrac{1}{2}}(1 + p\hat{P}\hat{\pi})\Phi_a \tilde{\Psi}_\Omega \,. \tag{2.8}$$

The diagonal matrix elements are

$$E^{\rm intr}_{\Omega p} = -\tfrac{1}{2}Ep\langle \tilde{\Psi}_\Omega | \hat{\pi} | \tilde{\Psi}_\Omega \rangle + \tilde{\varepsilon}_\Omega \,. \tag{2.9}$$

(v) An approximation to the operator $\hat{\pi}$ in the BCS 1-quasiparticle space is derived from the single-particle matrix elements

$$\hat{\pi} \to \sum_\Omega \langle \Psi_\Omega | \hat{\pi} | \Psi'_\Omega \rangle c^+_\Omega c'_\Omega \,. \tag{2.10}$$

Parity does not change under particle–hole conjugation so the result is

$$\langle \tilde{\Psi}_\Omega | \hat{\pi} | \tilde{\Psi}'_\Omega \rangle = (uu' + vv')\langle \Psi_\Omega | \hat{\pi} | \Psi'_\Omega \rangle \,. \tag{2.11}$$

(vi) After the matrix elements above have been evaluated, $\hat{H}_{\rm intr}$ can be constructed and diagonalized numerically.

(vii) The space of the total hamiltonian $\hat{H}$ is spanned by the symmetrized wave functions

$$\Psi^I_{\Omega p} = N(1 + \hat{R}_1) D^I_{m\Omega} \chi^{\rm intr}_{\Omega p} \,. \tag{2.12}$$

(viii) The formulae for the matrix elements of $\hat{H}_{\rm rotor}$ are identical with those for the standard BCS quasiparticle-plus-rotor hamiltonian [24]), except that the decoupling matrix elements between the $\hat{R}_1$ conjugate parts of the basis states $\Psi^I_{\Omega=1/2,p}$ must take into account symmetrization with respect to parity,

$$\langle \Psi_{1/2} | \hat{j}_+ | \hat{R}_1 \Psi'_{1/2} \rangle_{\rm rot} \to p \langle \hat{\pi} \Psi_{1/2} | \hat{j}_+ | R_1 \hat{\Psi}'_{1/2} \rangle_{\rm rot+oct} \,. \tag{2.13}$$

The final results are obtained by numerical diagonalization.

The strong coupling limit is used for comparison with experimental data in sect. 3. In this limit the off-diagonal matrix elements of $\hat{\pi}$ and $\hat{j}_+$ are mostly neglected, so no matrix diagonalization whatsoever is required after step (i) and the level energies are given by $E^{\rm intr}_{\Omega p}$ of eq. (2.9) plus the usual rotational model terms. Strong coupling to the reflection asymmetric deformation, i.e. neglect of the off-diagonal terms in step (vi), is justified if the term $\frac{1}{2}E\hat{\pi}$ is small compared to the energy separation of the parity-mixed Nilsson orbitals it connects. This is not always the case, because although the relevant single-particle orbitals are generally pushed apart by the octupole component of the single-particle potential, the Fermi level may lie between them so that their quasiparticle energies come close.

The diagonal matrix elements of $\hat{\pi}$ are analogous to the rotational $\Omega = \frac{1}{2}$ decoupling matrix elements. The parity splitting for pure strong coupling is simply

$$E\langle \Psi_\Omega | \hat{\pi} | \Psi_\Omega \rangle = E\left(\sum_{i^+} x^2_{i^+} - \sum_i x^2_i \right) , \tag{2.14}$$

where x_i^+ and x_i^- are the amplitudes of positive- and negative-parity components in the parity-mixed intrinsic orbital Ψ_Ω. For $\Omega = \frac{1}{2}$ the spectrum is complicated by the fact that the rotational decoupling factor of a given intrinsic orbital has opposite sign for positive and negative parity (eq. (2.13) above).

The full collective strength of odd-multipole electric operators goes within the strong-coupled parity doublet, just as the even-multipole collective strength goes within a rotational band. The dipole and octupole collective operators are

$$\hat{Q}_{10} = -\sqrt{3/4\pi} Z R_0 \varepsilon_1 , \tag{2.15}$$

$$\hat{Q}_{30} = -\tfrac{6}{7} Z R_0^3 \varepsilon_3 , \tag{2.16}$$

respectively. It is easily seen that

$$\langle \Psi^I_{\Omega p} | \hat{Q}_{30} | \Psi^I_{\Omega -p} \rangle = -\tfrac{6}{7} Z R_0^3 \bar{\varepsilon}_3 . \tag{2.17}$$

Generally, $\bar{\varepsilon}_3$ entails a displacement $\bar{\varepsilon}_1$ of the proton center of gravity, and

$$\langle \Psi^I_{\Omega p} | \hat{Q}_{10} p | \Psi^I_{\Omega -p} \rangle = -\sqrt{3/4\pi} Z R_0 \bar{\varepsilon}_1 . \tag{2.18}$$

A meaningful calculation of proton and neutron centers of gravity is difficult, so ε_1 will be determined phenomenologically and single-particle contributions to the E1 mode will not be evaluated in the reflection asymmetric basis. The evaluation of M1 matrix elements is standard [2,23], except that for $K = \frac{1}{2}$ the matrix elements of $\hat{s}_+$ and $\hat{l}_+$ must be modified in the same way as $\hat{j}_+$ in eq. (2.13).

2.3. INTERMEDIATE COUPLING

The starting point once more is

$$\hat{H} = \hat{H}_{\text{rotor}} + \hat{H}_{\text{intr}} . \tag{2.19}$$

A basis will be employed which is strong-coupled with respect to elongation, so that $\hat{H}_{\text{rotor}}$ is written in the same way as before, but weak-coupled with respect to reflection asymmetry so that $\hat{H}_{\text{intr}}$ is written

$$\hat{H}_{\text{intr}} = \hat{H}_{\text{core}} + [\hat{H}_{\text{s.p.}} + \hat{H}_{\text{pair}}]_{\varepsilon_3 = 0} + \hat{H}_{\text{coup}} . \tag{2.20}$$

The essential difference is that the folded Yukawa single-particle orbitals and the BCS transformation are computed for $\varepsilon_3 = 0$ and used to define a basis for diagonalization of the coupling to reflection asymmetry.

It is possible to have the same $\hat{H}_{\text{core}}$ as before – a static reflection asymmetric shape with parity splitting given by a parameter E. This is mathematically identical with a $K = 0$ vibrational core where all excited states except the 1-phonon level are truncated away, which is the case previously considered in the literature [e.g. refs. [16,25]]. A more general treatment is implemented below, where $\hat{H}_{\text{core}}$ is a

hamiltonian for one-dimensional anharmonic collective motion in the ε_3 degree of freedom,

$$H_{\text{core}} = -\frac{1}{2B}\frac{\mathrm{d}^2}{\mathrm{d}\varepsilon_3^2} + V(\varepsilon_3)\,. \tag{2.21}$$

If the extreme limit of adiabatic $K=0$ octupole collective motion were realized in nature it would be possible to calculate the inertial mass function $B(\varepsilon_3)$ and the potential energy function $V(\varepsilon_3)$ from the deformed shell model. Fig. 6 shows the

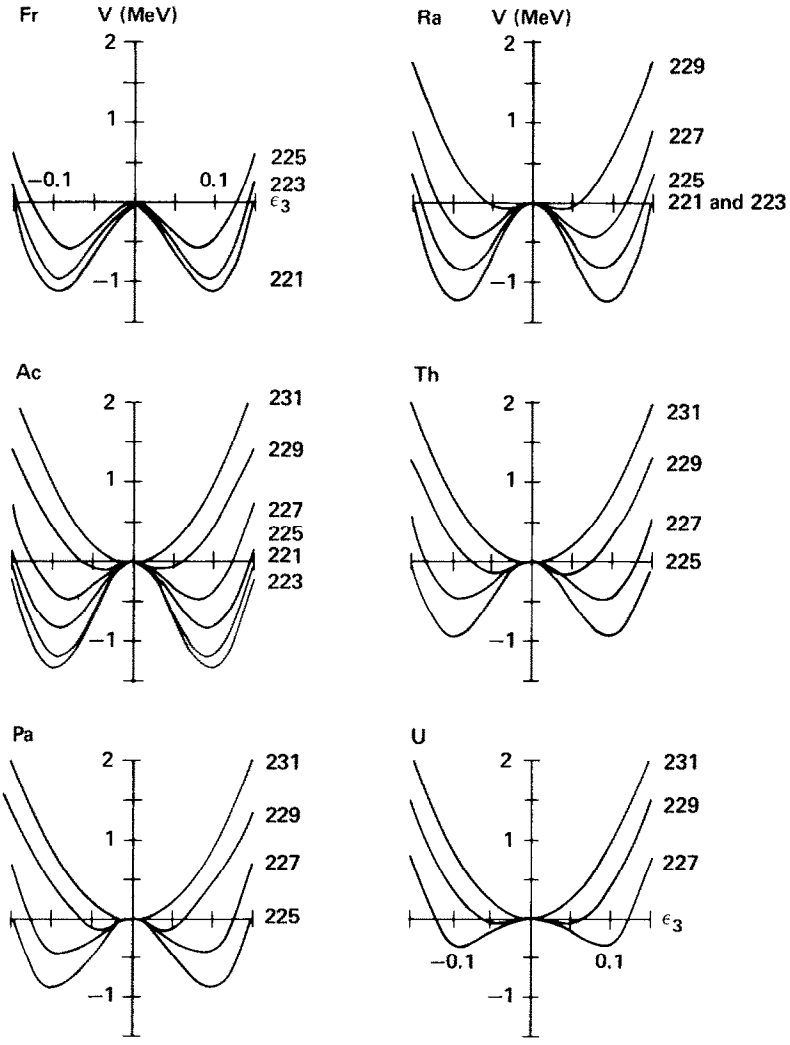

Fig. 6. The potential energy $V(\varepsilon_3)$ for the even cores of odd-A Fr-Ra-Ac-Th-Pa-U isotopes which are calculated to have ground-state octupole deformation. Each curve follows the appropriate [10]) minimal path in the ε_2, ε_4 plane.

potential curves $V(\varepsilon_3)$ from the folded Yukawa single-particle model for relevant odd-A cores. They are obtained by interpolation between neighboring even-A potential energy curves, after minimization with respect to ε and ε_4. Microscopic calculations of the inertial mass function will be deferred to a future paper. *A priori*, it may be suspected that an effective B (and maybe V) must be employed to absorb extraneous effects. For example, coupling to the $K \neq 0$ octupole modes is estimated to have a large effect on both the ground-state parity splitting [26]) and the $K = 0$ excited levels [27]). Therefore the inertial mass function B will presently be handled in the same way as the parity-splitting parameter E of strong coupling and the rotational inertia $\mathcal{I}$. It is assigned a constant value which is adjusted to reproduce the parity splitting in neighboring doubly even nuclei. A general dynamical Bohr hamiltonian for the quadrupole and octupole modes was recently formulated by Rohozinski *et al.* [28]).

The core-particle coupling cannot be given analytical form in a numerical single-particle potential like the folded Yukawa. It could be extracted numerically, but here it is approximated by

$$\hat{H}_{\text{coup}} = k\hbar\omega_0 R^{-1} r^3 P_3(\cos\theta)\varepsilon_3 , \tag{2.22}$$

where r, θ are Nilsson's stretched coordinates [14]) and R is in oscillator units so that k is of order unity. The pairing factor on $\hat{H}_{\text{coup}}$ after a BCS transformation is $uu' - vv'$.

The solution of the intermediate coupling hamiltonian proceeds in the following steps:

(i) $\hat{H}_{\text{s.p.}}$ is diagonalized for $\varepsilon_3 = 0$ to give ε_Ω and Ψ_Ω.

(ii) A set of states near the fermi level is selected to define the single-particle space of the coupling calculation.

(iii) A coupling constant k is now determined which is appropriate for this truncated space and the approximation (2.22): $[H_{\text{s.p.}}]_{\varepsilon_3=0} + \hat{H}_{\text{coup}}(\varepsilon_3)$ is diagonalized for a sequence of ε_3 values and k is chosen to optimize the agreement with the folded Yukawa single-particle energies as a function of ε_3.

(iv) $\hat{H}_{\text{pair}}$ is diagonalized by a BCS transformation to give $\tilde{\varepsilon}_\Omega$ and $\tilde{\Psi}_\Omega$.

(v) $\hat{H}_{\text{core}}$ is diagonalized in a harmonic oscillator basis to give energies E_{n_3} and wave functions ϕ_{n_3}, $n_3 = 0, 1, 2, \ldots$, which are eigenstates of both $\hat{R}_1$ and the core-parity operator $\hat{P}$ with the same eigenvalue $(-)^{n_3}$.

(vi) $\hat{H}$ is diagonalized in the basis

$$N(1 + \hat{R}_1) D^I_{M\Omega} \tilde{\Psi}_\Omega \phi_{n_3} . \tag{2.23}$$

A dipole collective operator is needed for the evaluation of E1 transition matrix elements. It can be obtained phenomenologically [16]) by taking ε_1 of eq. (2.15) as a dynamical variable proportional to ε_3. Matrix elements of the electromagnetic operators are standard [2,23]), except for the additional phase $(-)^{n_3}$ on $\hat{R}_1$ conjugate components.

2.4. COMPARISON OF INTERMEDIATE AND STRONG COUPLING

Differences between intermediate- and strong-coupling calculations for the same nucleus may arise because:

(i) Higher $K=0$ octupole excitations, above the first $K^\pi = 0^\pm$ pair, are sometimes important in intermediate coupling but are not included in the strong coupling core space. The example of the soft nucleus ^{229}Th is studied in sect. 4.

(ii) The single-particle space of intermediate coupling is generally, though not necessarily, truncated to include just a few single-particle states near the Fermi level at $\varepsilon_3 = 0$. There are usually large octupole matrix elements out of such a basis space, which are automatically incorporated in step (i) of strong coupling. However, the effect of doubling the intermediate-coupling basis space was checked for the ^{229}Th calculation below, and an odd-proton case, and proved to be insignificant for the low-energy spectrum.

(iii) The single-particle response to reflection asymmetry in the present work is derived somewhat differently for intermediate and strong coupling (cf. the discussion of $\hat{H}_{\text{coup}}$ in subsect. 2.3). The combined error due to this approximation and single-particle truncation shows up when step (iii) of subsect. 2.3 is carried out. For the ^{229}Th case it was not negligible, but no larger than the probable error relative to experiment due to the inherent inaccuracy of single-particle energies in the deformed shell model [20]).

(iv) The fact that the BCS transformation is carried out at $\varepsilon_3 = 0$ for intermediate coupling, but at $\varepsilon_3 = \bar{\varepsilon}_3$ for strong coupling, introduces a basic difference between the two schemes. In the quadrupole case this difference is sometimes crucial for energy spectra [for example, the "$j-1$ effect" [29])] and for wave functions (for example, the spectroscopic factor of $d_{3/2}$, $I = \frac{1}{2}$ states). The remaining part of this subsection describes a simple analytical model which nevertheless incorporates the main characteristics of octupole deformed systems. It will be possible to compare the BCS effects in intermediate versus strong coupling and to specify the nature of the difference that arises.

First the solvable model is outlined without pairing. A reader who is uneasy about the claim that the intermediate-coupling and strong-coupling formalisms of subsects. 2.2 and 2.3 are identical, apart from the technicalities just mentioned, may find it helpful to work through this part in detail. It illustrates the role of coupling to the reflection asymmetry in the weak-coupling basis, or equivalently the role of decoupling in the strong-coupling basis.

The basic ingredients of the model are: a two-dimensional core space spanning the $K^\pi = 0^+$ and 0^- configurations observed in doubly even nuclei, and a two-dimensional single-particle space for given Ω illustrated in fig. 7, or trivially several such pairs of single-particle levels for different Ω.

The single-particle states $|1\rangle_0$ and $|2\rangle_0$ at $\varepsilon_3 = 0$ are used for intermediate coupling. They have good parity $-\pi$ and π, and single-particle energies e_0 and $-e_0$, respec-

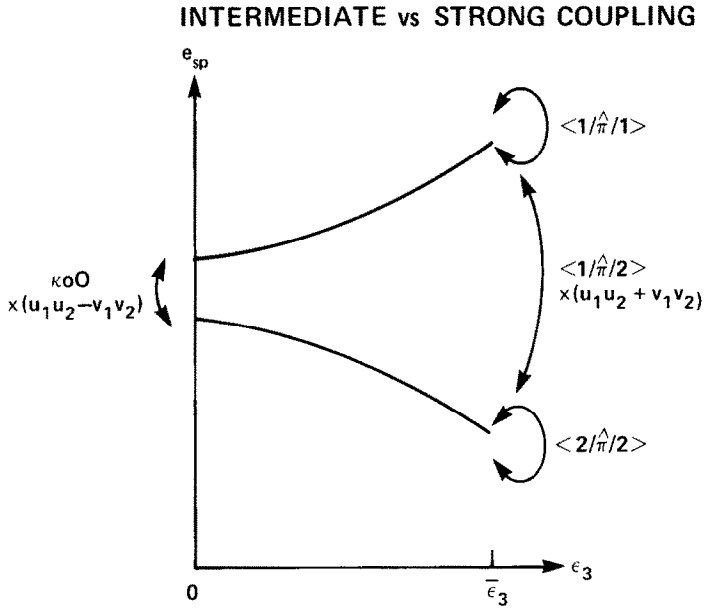

Fig. 7. Two single-particle orbitals, $|1\rangle$ and $|2\rangle$, which constitute the single-particle space of the analytical model in subsect. 2.4, plotted as a function of ε_3. At $\varepsilon_3=0$ their parities are $-\pi$ and π, respectively ($\pi=\pm1$). The octupole-octupole coupling κoO is denoted V in the text. The energy splitting is denoted $2e_0$ at $\varepsilon_3=0$, and $2e=2(e_0^2+V^2)^{1/2}$ at $\varepsilon_3=\bar{\varepsilon}_3$.

tively. The energies of the core states $|0^+\rangle$ and $|0^-\rangle$ are denoted $-C$ and C. (Note that the core parity splitting is $2C$, equal to the parameter E above.) The core-particle octupole interaction matrix element κoO will be written V for short. The hamiltonian matrix for $I=\Omega$, with basis states indicated to the right, is then

$$\hat{H}=\begin{pmatrix} e_0+C & V & 0 & 0 \\ V & -e_0-C & 0 & 0 \\ 0 & 0 & e_0-C & V \\ 0 & 0 & V & -e_0+C \end{pmatrix}, \quad \begin{matrix} |1\rangle_0|0^-\rangle \\ |2\rangle_0|0^+\rangle \\ |1\rangle_0|0^+\rangle \\ |2\rangle_0|0^-\rangle \end{matrix} \quad \begin{matrix} \} \, p=\pi \\ \\ \} \, p=-\pi \end{matrix}. \tag{2.24}$$

In strong coupling the core-particle octupole interaction is first diagonalized in the single-particle space

$$\hat{H}_{\text{s.p.}}=\begin{pmatrix} e_0 & V \\ V & -e_0 \end{pmatrix}, \quad \begin{matrix} |1\rangle_0 \\ |2\rangle_0 \end{matrix}. \tag{2.25}$$

The eigenstates $|1\rangle$ and $|2\rangle$ have energies $\pm\sqrt{e_0^2+V^2}$, henceforth denoted $\pm e$ for short. The parity operator

$$\hat{\pi}=\begin{pmatrix} -\pi & 0 \\ 0 & \pi \end{pmatrix}, \quad \begin{matrix} |1\rangle_0 \\ |2\rangle_0 \end{matrix}, \tag{2.26}$$

transforms into

$$\hat{\pi} = \frac{\pi}{e}\begin{pmatrix} -e_0 & -V \\ -V & e_0 \end{pmatrix}, \qquad \begin{matrix} |1\rangle \\ |2\rangle \end{matrix}. \tag{2.27}$$

The states $|1\rangle$ and $|2\rangle$ are coupled to the core state $|\phi_a\rangle$ of subsect. 2.2 and symmetrized to good parity p. The strong-coupling hamiltonian becomes

$$\hat{H} = \begin{pmatrix} e+\frac{e_0 C}{e} & \frac{VC}{e} & 0 & 0 \\ \frac{VC}{e} & -e-\frac{e_0 C}{e} & 0 & 0 \\ 0 & 0 & e-\frac{e_0 C}{e} & \frac{-VC}{e} \\ 0 & 0 & \frac{-VC}{e} & -e+\frac{e_0 C}{e} \end{pmatrix}, \qquad \begin{matrix} |1, p=\pi\rangle \\ |2, p=\pi\rangle \\ |1, p=-\pi\rangle \\ |2, p=-\pi\rangle \end{matrix}, \tag{2.28}$$

The collective E3 operator normalized to unit strength should obviously be

$$\hat{M}(\mathrm{E3}) = \begin{pmatrix} 0 & 0 & 1 & 0 \\ 0 & 0 & 0 & 1 \\ 1 & 0 & 0 & 0 \\ 0 & 1 & 0 & 0 \end{pmatrix} \tag{2.29}$$

in either one of the basis representations.

Now it is a straightforward exercise to verify that:

(i) The energy spectrum is identical for the two coupling schemes. Notably [10]), the parity splitting in the odd-A nucleus is reduced relative to the core for $V \neq 0$, and it goes to zero if $e_0 \to 0$, $C \to 0$ or $V \to \infty$.

(ii) The wave functions are identical, if the core basis states of strong coupling may be related to those of intermediate coupling by symmetrization

$$|0^{\pm}\rangle = \sqrt{\tfrac{1}{2}}(|\phi_a\rangle \pm |\phi_b\rangle)\,. \tag{2.30}$$

(iii) The E3 transition rates obtained with the operator (2.29) are identical in both schemes. Within the lowest parity doublet, letting $e_0 \to 0$ to simplify the expressions, the result is

$$\frac{\langle p=\pi|\hat{M}(\mathrm{E3})|p=-\pi\rangle}{\langle 0^+|\hat{M}(\mathrm{E3})|0^-\rangle} = \frac{V}{\sqrt{C^2+V^2}} \tag{2.31}$$

which approaches the full collective strength only for $V \gg C$. For $V=0$ it is 0, reflecting the fact that the lowest parity doublet consists of two reflection symmetric single-particle states which are "accidentally" closely spaced (since we let $e_0 \to 0$ in eq. (2.31)). Then the collective E3 strength from each state goes to the octupole

excitation at $2C$, the same energy as in the core. For the same core and different $\Omega^{\pm\pi}$ single-particle pairs, all intermediate situations may occur.

To introduce BCS pairing, a Fermi level λ and a gap parameter Δ are assumed. The single-particle energies are eplaced by quasiparticle energies,

$$\tilde{e}_{1,2} = \{(\lambda \mp e_0)^2 + \Delta^2\}^{1/2}, \tag{2.32}$$

or e instead of e_0 on the right-hand side for strong coupling. It is convenient to translate the energy scale by defining the quasiparticle energies as

$$\pm\delta_0 \equiv \pm(\tilde{e}_2 - \tilde{e}_1), \tag{2.33}$$

or δ for strong coupling. The intermediate-coupling hamiltonian is

$$\hat{H} = \begin{pmatrix} \delta_0 + C & V(u_1u_2 - v_1v_2) & 0 & 0 \\ V(u_1u_2 - v_1v_2) & -\delta_0 - C & 0 & 0 \\ 0 & 0 & \delta_0 - C & V(u_1u_2 - v_1v_2) \\ 0 & 0 & V(u_1u_2 - v_1v_2) & -\delta_0 + C \end{pmatrix}. \tag{2.34}$$

The pairing occupation amplitudes are

$$v_{1,2} = [\tfrac{1}{2}(1 + (\lambda \mp e_0)/\tilde{e}_{1,2})]^{1/2},$$
$$u_{1,2} = [1 - v_{1,2}^2]^{1/2}, \tag{2.35}$$

or e instead of e_0 on the right-hand side for strong coupling. The strong-coupling hamiltonian is

$$\hat{H} = \begin{pmatrix} \delta + \dfrac{e_0 C}{e} & \dfrac{VC}{e}(u_1u_2 + v_1v_2) & 0 & 0 \\ \dfrac{VC}{e}(u_1u_2 + v_1v_2) & -\delta - \dfrac{e_0 C}{e} & 0 & 0 \\ 0 & 0 & \delta - \dfrac{e_0 C}{e} & \dfrac{-VC}{e}(u_1u_2 + v_1v_2) \\ 0 & 0 & \dfrac{-VC}{e}(u_1u_2 + v_1v_2) & -\delta + \dfrac{e_0 C}{e} \end{pmatrix}. \tag{2.36}$$

Insertion of realistic numbers shows that the intermediate- and strong-coupling schemes are *not* equivalent, except of course when $V \to 0$ or $\lambda \to \pm\infty$. However, in most cases the results seem to be very similar.

The special case $\lambda = 0$, i.e. with the Fermi level halfway between the single-particle levels, is interesting because the effects of pairing are expected to be maximal. Furthermore, since the quasiparticle states are degenerate ($\delta = 0$) for $\varepsilon_3 \neq 0$ as well as $\varepsilon_3 = 0$, the effect of the off-diagonal term in the strong-coupling representation is maximal. For intermediate coupling the solution is trivial since $\delta_0 = 0$ and $u_1u_2 -$

$v_1 v_2 = 0$. The ground state is an exactly degenerate parity doublet, and there is no collective E3 strength within the doublet since it corresponds to "accidentally" degenerate quasiparticles. The E3 strength goes to the second parity doublet which lies $2C$ up in energy, corresponding to the core octupole excitation. For strong coupling the results are similar. There are two exactly degenerate parity doublets. The collective E3 strength within each doublet is exactly zero, seemingly a complete breakdown of strong coupling, and the full octupole strength goes to a state in the other doublet. The only difference compared to intermediate coupling lies in the excitation energy of the octupole excited doublet, which is

$$2C\sqrt{\frac{e_0^2 + V^2\Delta^2/(e^2+\Delta^2)}{e_0^2 + V^2}}, \tag{2.37}$$

reduced from the intermediate-coupling value $2C$ by a square root factor which is less than or equal to one. In conclusion, with the Fermi level halfway between the single-particle levels, the odd-A octupole mode decouples. The octupole excitation energy of the decoupled mode is equal to the core value in intermediate-coupling theory, but in strong-coupling it is reduced by the factor (2.37) which goes to zero in the limit $V \gg e_0, \Delta$.

3. Evidence for parity-mixed intrinsic orbitals

3.1. QUASIPARTICLE ENERGY LEVELS

The signature of $C_{\infty h}$ octupole shapes suggested by molecular spectroscopy is parity doubling, i.e. for each band head there should be another band head close in energy with the same K but opposite parity. According to the strong-coupling model in subsect. 2.3, or the analytical model in subsect. 2.4, the energy splitting should always be smaller in odd-A than in doubly even nuclei. Since the parity-doubling criterion has frequently been invoked in the literature it is perhaps in place to emphasize three *negative* statements:

(i) It is a necessary but *not* sufficient criterion for octupole deformation.

(ii) The size of the energy splitting in a doublet does *not* provide a useful measure of the amount of octupole deformation nor its stability, even if an octupole connection can be inferred in other ways.

These two statements are general and follow from any of the models in sect. 2. Furthermore, case studies of individual nuclei show that:

(iii) Parity doubling and splitting is *not* a useful criterion by itself for inferences about the octupole mode in odd-A nuclei of the actinium region.

The reason is well known: there "happen" to be many closely spaced parity doublets among the Nilsson orbitals in the deformed shell model for reflection symmetric shapes, both for neutrons and protons [refs. [6,20]), figs. 2, 3]. These pairs of Nilsson orbitals run almost parallel as a function of ε_2, they actually cross in

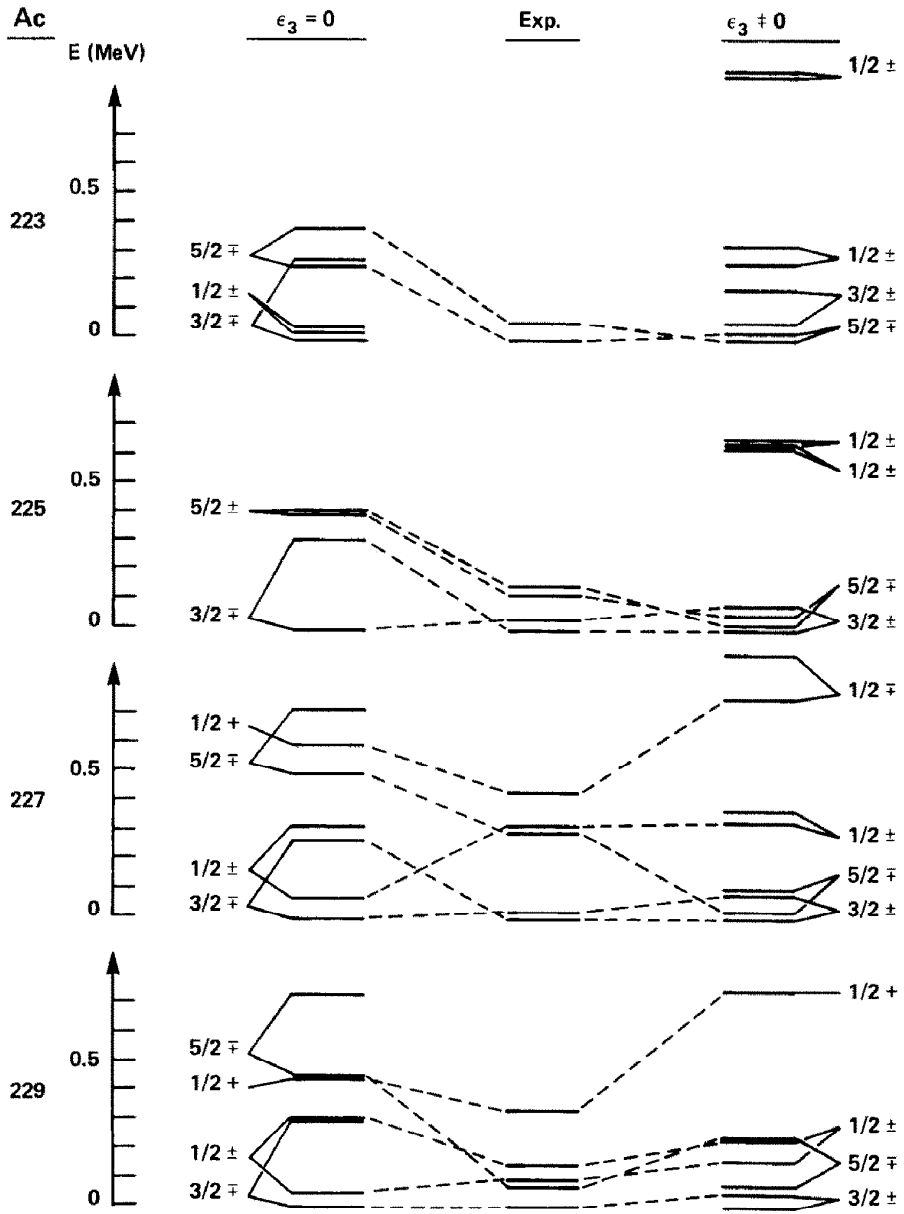

Fig. 8. Nilsson quasiparticle levels in the odd-mass actinium isotopes. The experimental levels (middle) are compared with levels derived from the folded Yukawa model (right) and levels derived under the constraint $\varepsilon_3 = 0$ (left). The agreement in either case is about equally good, and as good as in the heavier actinides where the folded Yukawa parameters were fitted [20]). Note that the parity splitting is smaller for $\varepsilon_3 = 0$ than for $\varepsilon_3 \neq 0$ in the $\frac{5}{2}$ doublet of ^{225}Ac.

some places, and the spacing of quasiparticle levels is further reduced by pairing especially when the Fermi level lies between the single-particle levels.

A systematic comparison with experiment of reflection symmetric and asymmetric Nilsson quasiparticle levels is shown for the actinium isotopes in fig. 8. Each asymmetric Nilsson orbital ($\varepsilon_3 \neq 0$) is represented by a parity doublet whose splitting is calculated in the strong-coupling limit of subsect. 2.2. On the symmetric side ($\varepsilon_3 = 0$) in fig. 8, pairs of Nilsson orbitals have been connected into doublets although this is completely arbitrary. The equilibrium ε and ε_4 deformations of the potential-energy surfaces are employed, and standard BCS pairing is used, so no adjustable parameters have been introduced to fit these odd-A data.

Fig. 8 illustrates points (i)–(iii) above. The experimental band-head energies in the whole sequence of actinium isotopes is about *equally well* described by the folded Yukawa model at $\varepsilon_3 = 0$ and $\varepsilon_3 \neq 0$. The energy splitting in some parity doublets, for example $\frac{5}{2}^{\pm}$ in ^{225}Ac, comes out *smaller* for $\varepsilon_3 = 0$ than it does either for $\varepsilon_3 \neq 0$ or experiment. The implication for a near-degenerate $\frac{5}{2}^{\pm}$ ground-state doublet recently reported [12]) in ^{229}Pa is that the primary evidence for an octupole connection does not come from the small energy splitting *per se*, but from the agreement with a theoretical calculation [18]) that was carefully tuned to empirical data in slightly heavier isotopes and simultaneously predicts the octupole connection. A crucial experimental test is suggested in subsect. 3.3 below.

A case where octupole deformation does significantly improve the quasiparticle level scheme has been provided by recent measurements on the ^{225}Ra nucleus [30]). Fig. 9 compares the experimental levels with the theoretical ones at the constrained equilibrium deformation for $\varepsilon_3 = 0$ ($\varepsilon = 0.14$) and the true equilibrium at $\varepsilon_3 = 0.1$, respectively. At $\varepsilon_3 = 0$ the nearest candidate for the $\frac{1}{2}^{+}$ ground state lies 850 keV above the lowest quasiparticle state (cf. fig. 2). At $\varepsilon_3 = 0.1$, on the other hand, an $\Omega = \frac{1}{2}$ parity-mixed Nilsson orbital at the $N = 137$ Fermi level accounts for the $\frac{1}{2}^{\pm}$ ground-state doublet in ^{225}Ra (figs. 4 and 9). An ε_3 deformation at least this large is required not only for the quasiparticle energy but also for $\langle \hat{\pi} \rangle$ to have the right sign. The structure of the wave function is discussed in the following subsection.

3.2. DECOUPLING FACTORS

The decoupling parameter a is an intrinsic single-particle matrix element which can easily be extracted from the experimental energies in a $K = \frac{1}{2}$ band by fitting to the rotational model formula [2])

$$E_I = A[I(I+1) + a(-)^{I+1/2}(I+\tfrac{1}{2})] + \cdots . \tag{3.1}$$

For a weak-coupling basis state (2.23)

$$a = -(-)^{n_3} \langle \Psi_{1/2} | \hat{j}_+ | \hat{R}_1 \Psi_{1/2} \rangle , \tag{3.2}$$

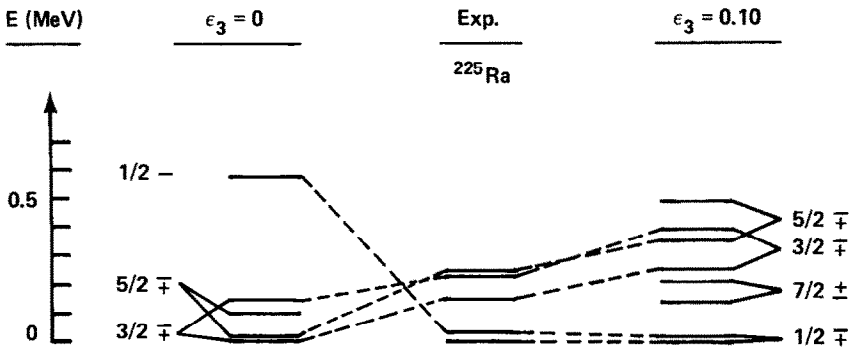

Fig. 9. Same as fig. 8, but for ^{225}Ra. The $\frac{1}{2}^+$ ground state can only be accounted for with octupole deformation. Furthermore, the $\frac{1}{2}^-$ decoupling factor from experiment matches theory only with the inclusion of octupole deformation (table 2b).

and for a strong-coupling basis state (2.12)

$$a = -p\langle \hat{\pi}\Psi_{1/2}|\hat{j}_+|\hat{R}_1\Psi_{1/2}\rangle . \tag{3.3}$$

In both cases, opposite-parity states of a doublet have decoupling factors of equal magnitude but opposite sign. This signature of the octupole mode has been verified in octupole vibrational nuclei [2]).

The observation of decoupling factors of opposite sign in a $K = \frac{1}{2}$ parity doublet thus indicates that the octupole mode and only one Nilsson orbital are involved, but gives no indication as to the character of the octupole mode. A simultaneous reduction of the energy splitting between the band heads relative to the doubly even neighbors does, however, suggest that the octupole interaction mixes intrinsic single-particle states of different parity. Further evidence for a parity-mixed single-particle state might be found in a deviation of the decoupling factor from experimental systematics, or from the theoretical value at $\epsilon_3 = 0$.

Evidence for strong coupling to the octuple mode, or a quantitative measure of the approach to the strong-coupling limit can be obtained under favorable circumstances. We note that when reflection symmetric Nilsson orbitals of different parity are mixed, the quantity which hybridizes and averages out is actually the decoupling factor times the parity, henceforth referred to as the decoupling invariant. Thus a favorable situation is at hand when an observed $K^\pi = \frac{1}{2}^\pm$ doublet might be accounted for either by two reflection symmetric Nilsson orbitals with widely different decoupling invariants, or alternatively by a single strong-coupled Nilsson orbital resulting from the mixing of the two symmetric ones. The degree to which the observed decoupling invariants in the $K = \frac{1}{2}^\pm$ doublet approach a common intermediate value measures the degree of approach to the strong-coupling limit.

Experimental decoupling invariants are listed in tables 2a,b for proposed octupole transitional and deformed nuclei. The tables include theoretical values for the Nilsson orbitals which are calculated to lie closest to the Fermi level; the reflection symmetric

case to the left and the asymmetric case to the right. In ^{227}Ac the experimental decoupling invariants for $[660]\frac{1}{2}$ and $[530]\frac{1}{2}$ are closer together than the theoretical values at $\varepsilon_3 = 0$, but the coupling to the octupole is not very strong. Significantly, the energy splitting of the $K^\pi = \frac{1}{2}^\pm$ doublet is reduced only by a factor of two relative to the doubly even neighbors [31]). The approach to strong coupling is seen to be more nearly complete in the observed $K^\pi = \frac{1}{2}^\pm$ doublet of the nucleus ^{225}Ra. The $\varepsilon_3 \neq 0$ decoupling invariant in table 2b for both ^{223}Ra and ^{225}Ra is a rapidly decreasing function of ε_3 near the calculated equilibrium, $\varepsilon_3 \sim 0.1$, because the component of $[640]\frac{1}{2}$ is increasing. The fact that the experimental value in ^{225}Ra is on the small side may thus be taken to indicate that the octupole deformation is at least this large.

The octupole mixing of $K = \frac{1}{2}$ orbitals in ^{227}Ra is relatively complex. Notably, strong coupling to the octupole deformation accounts for the anomalous positive sign of the decoupling invariant for $[631]\frac{1}{2}$ and its octupole band. Reflection symmetric theory and the systematic empirical trend from heavier nuclei [22]) both point

TABLE 2a

The decoupling parameter (a) times the parity (p) for $K = \frac{1}{2}$ bands in the $_{89}$Ac isotopes

Nucleus	p	Label		ap		
		$\varepsilon_3 = 0$	$\varepsilon_3 \neq 0$	$\varepsilon_3 = 0$	exp	$\varepsilon_3 \neq 0$
^{221}Ac	+	640	541	6.7		−2.4
	−	530		2.8		
^{223}Ac	+	640	541	6.5		−1.8
	−	530		2.3		
^{225}Ac	+	640		6.4		2.3
	−	530		2.2		
	+		541			−1.2
	−					
^{227}Ac	+	660		5.9	4.6	3.1
	−	530		1.8	2.2	
	+	400		0.6	0.7	0.3
	−					
^{229}Ac	+	660		4.8		3.3
	−	530		1.8	>0	
	+	400		1.8	≳0	1.0
	−					

The experimental bands are assigned in the Table of isotopes [6]), except the $[660]\frac{1}{2}$ assignment which was made [31]) on the basis of recent measurements [32,33]). Theoretical values are calculated at the equilibrium values [10]) of ε_2, ε_4 and, for the column furthest to the right, ε_3 (fig. 6).

TABLE 2b

Same as table 2a but for odd-neutron $K=\frac{1}{2}$ bands in isotopes of $_{88}$Ra

Nucleus	p	Label		ap		
		$\varepsilon_3=0$	$\varepsilon_3\neq 0$	$\varepsilon_3=0$	exp	$\varepsilon_3\neq 0$
^{221}Ra	+	640	651	−0.3		−3.5
	−	770		7.7		
^{223}Ra	+	640		0.1		2.7 [a]
	−	770		7.5		
^{225}Ra	+	640		−0.1	1.5	2.8 [a]
	+	631		0.4		
	−	770		7.0	2.4	
^{227}Ra	+	631		−0.1	1.5	1.1
	−				1.8	
	+					4.1
	−	761		3.9	4.3	
	+					−0.9
	−	501		2.1	−0.9	

The experimental data are from ref. [30]) for ^{225}Ra and ref. [36]) for ^{227}Ra.
[a]) Rapidly decreasing as a function of ε_3.

to a negative decoupling invariant for $[631]\frac{1}{2}$. Equal success in this respect, and a good overall description of the low-lying bands in ^{227}Ra, was also obtained in the intermediate coupling model using the soft octupole deformed potential in fig. 6 and a fairly large single-particle space. Octupole deformation is also consistent with the conventional negative sign of the decoupling invariant for $[501]\frac{1}{2}$. For $\varepsilon_3=0$, on the other hand the $[501]\frac{1}{2}$ orbital mixes with $[770]\frac{1}{2}$ specifically at the quadrupole deformation of ^{227}Ra (fig. 2) and acquires a positive decoupling invariant.

Spectroscopic studies of lighter isotopes might well prove interesting. The potentials in fig. 6 suggest that the parity doublet discussed above for ^{227}Ac might come closer to the strong coupled limit in ^{225}Ac. In ^{221,223}Ac there is the possibility of observing a Nilsson orbital with a large component of $[541]\frac{1}{2}$ and a *negative* decoupling invariant, which would be brought into the vicinity of the Fermi level specifically due to octupole deformation. Similarly, the observation of a negative decoupling invariant in ^{221}Ra due to $[651]\frac{1}{2}$ would be positive evidence for octupole deformation.

3.3. M1 PROPERTIES

Magnetic dipole moments and gyromagnetic factors hybridize when reflection symmetric Nilsson orbitals are mixed by octupole deformation, just like the decoupling invariants in the previous subsection. The usual formulae [14]) can be used to calculate μ and g_K for intrinsically parity-mixed Nilsson states, except that the

magnetic decoupling factor is modified in analogy with eq. (2.13) for the rotational decoupling factor. From the expression for g_K,

$$g_K = \frac{1}{K}\{Kg_l + (g_s - g_l)\langle \Psi_K | \hat{s}_z | \Psi_K \rangle\}, \tag{3.4}$$

it is clear that the hybridization of magnetic dipole properties due to octupole deformation is most conspicuous when spin-flipped orbitals are mixed. Near the proton Fermi level in the actinium region there are two such pairs of spin-flipped orbitals which interact strongly through a Y_{30} field component: $[532\downarrow]^3_2$ with $[651\uparrow]^3_2$ and $[523\downarrow]^5_2$ with $[642\uparrow]^5_2$. The expectation value of $\hat{s}_z$ for these orbitals under constraint of reflection symmetry is indicated by the dashed curves in fig. 10. The

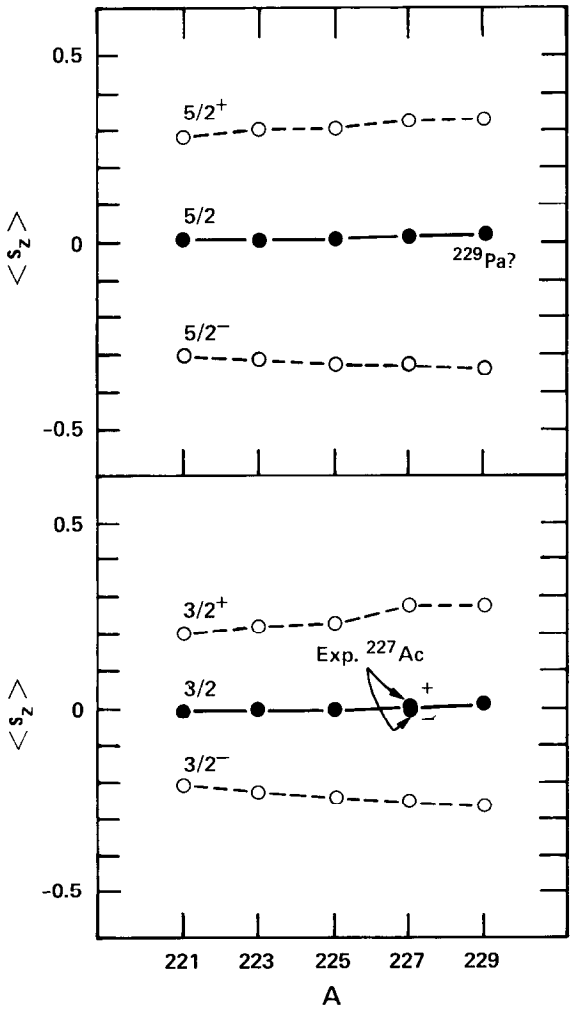

Fig. 10. The $\langle \hat{s}_z \rangle$ for the $\frac{3}{2}^{\pm}$ and the $\frac{5}{2}^{\mp}$ doublets observed or expected at low energy in odd-mass isotopes of Ac and Pa, calculated for $\varepsilon_3 = 0$ (open circles) and $\varepsilon_3 \neq 0$ (filled circles). Experimental data for ^{227}Ac indicate that the ground-state $\frac{3}{2}^{\pm}$ doublet stems from a single parity-mixed Nilsson orbital.

hybridized value for the parity-mixed orbital of the same K near the Fermi level at the asymmetric equilibrium shape is indicated by a solid curve.

Experimentally, the $\langle \hat{s}_z \rangle$ can be extracted by measuring the magnetic moment, or by measuring E2/M1 mixing or branching ratios within the rotational band, if the core intrinsic quadrupole moment is known and the core and single-nucleon effective g-factors can be adequately estimated [2]). Fig. 10 shows the values extracted from experiment [31,32]) for the $\frac{3}{2}^{\pm}$ bands of ^{227}Ac. The experimental points almost coincide, as they should if the ground-state $\frac{3}{2}^{\pm}$ doublet of ^{227}Ac stems from a single parity-mixed Nilsson orbit coupled adiabatically to octupole deformation in the intrinsic frame.

Similar measurements for ^{229}Pa could experimentally establish a corresponding assignment to the ground-state $\frac{5}{2}^{\pm}$ doublet [12]). A strong octupole coupling for both the ^{227}Ac, $\frac{3}{2}^{\pm}$ and the ^{229}Pa, $\frac{5}{2}^{\pm}$ ground-state doublets was obtained in a calculation by Chasman [18]), and the former prediction can be regarded as borne out by the data points in fig. 10.

TABLE 3

Experiment versus theory at $\varepsilon_3=0$ and $\varepsilon_3\neq 0$ for the ground-state spin, parity and magnetic moment of odd-A radium nuclei

Nucleus	I^p_{exp}	μ_{exp}	I^p_{th}	μ_{th}	ε_3	Configuration
^{221}Ra	$\frac{5}{2}$	−0.18	$\frac{5}{2}^{(+)}$ [a])	−0.13	0.10	$[642]\otimes[752]^{\frac{5}{2}}_{\frac{5}{2}}$
			$(\frac{5}{2}^{+}$	0.39	0	$[633]^{\frac{5}{2}}_{\frac{5}{2}})$ [b])
^{223}Ra	$\frac{3}{2}$	+0.28	$\frac{3}{2}^{+}$	0.50 [c])	0.10	$[642]^{\frac{3}{2}}_{\frac{3}{2}}$
			$\frac{3}{2}^{+}$	0.03	0	$[631]^{\frac{3}{2}}_{\frac{3}{2}}$
			$\frac{3}{2}^{-}$	−0.06	0	$[761]^{\frac{3}{2}}_{\frac{3}{2}}$ [d])
^{225}Ra	$\frac{1}{2}^{+}$	−0.75	$\frac{1}{2}^{+}$	−0.75 [e])	0.1 [e])	$[640]^{\frac{1}{2}}_{\frac{1}{2}}\otimes\cdots$
			(			$)$ [f])
^{227}Ra	$\frac{3}{2}^{+}$	−0.41	$\frac{3}{2}^{+}$	−0.41 [g])	0.08	$[631]^{\frac{3}{2}}_{\frac{3}{2}}$
			$\frac{3}{2}^{+}$	−0.06	0	$[631]^{\frac{3}{2}}_{\frac{3}{2}}$
^{229}Ra	$\frac{5}{2}$	+0.51	$\frac{5}{2}^{+}$	0.38	0.04	$[633]^{\frac{5}{2}}_{\frac{5}{2}}$
			$\frac{5}{2}^{+}$	0.61	0	$[633]^{\frac{5}{2}}_{\frac{5}{2}}$
			$\frac{5}{2}^{-}$	−0.29	0	$[752]^{\frac{5}{2}}_{\frac{5}{2}}$ [d])

The experimental spins and moments are from recent laser measurements [34]). The theoretical magnetic moments are obtained with $g_s/g_s^{free}=0.7$ and $g_R=Z/A$. Calculated ground-state values are given both for the equilibrium ε_3 deformation and for $\varepsilon_3=0$. Theory is compatible with experiment at the octupole deformed equilibrium points, but not at $\varepsilon_3=0$ in all cases.

[a]) The $\langle \hat{\pi} \rangle$ is very small.

[b]) Far from the lowest quasiparticle level at this deformation.

[c]) $\mu_{th}=\mu_{exp}$ if there is a 3% Coriolis admixture of $[651]^{\frac{1}{2}}_{\frac{1}{2}}$.

[d]) Near the lowest quasiparticle level at this deformation.

[e]) μ_{th} is sensitive to ε_3.

[f]) No candidates at $\varepsilon_3=0$, see subsect. 3.1.

[g]) Includes the effect of a realistic ~1% Coriolis admixture.

In the odd-neutron $^{221-229}$Ra nuclei, the ground-state spins and magnetic moments have recently been determined by laser measurements [34]). The data are shown in table 3 and compared with theory at $\varepsilon_3 = 0$ and $\varepsilon_3 \neq 0$. All the experimental results are consistent with the calculated $\varepsilon_3 \neq 0$ equilibrium points. The remainder of this subsection substantiates this main conclusion with a detailed discussion of the items in table 3.

The magnetic decoupling factors of the $K = \frac{1}{2}$ bands are expected to hybridize to the same extent as the rotational decoupling factors discussed above. Consequently the magnetic moment of the $\frac{1}{2}^+$ ground state in ^{225}Ra is calculated to be a rapidly changing function of ε_3 around the equilibrium value, $\varepsilon_3 \simeq 0.1$, like the decoupling factor. The experimental value, $\mu \simeq -0.75$ n.m., does in fact coincide with the theoretical value at ε_3 slightly larger than 0.1, just like the parity splitting and the decoupling factor (subsects. 3.1 and 3.2). The calculations suggest that the same orbital could be observed in ^{223}Ra. For ^{221}Ra, table 2b above includes a different $K = \frac{1}{2}$ orbital which might be observed in the excitation spectrum ($\varepsilon_2 = 0.10$ in fig. 4). The calculated band-head I^π is $\frac{3}{2}^+$ and the magnetic moment is $\mu \simeq 0.4$, incidentally similar to that of a nearby $K = \frac{3}{2}$ orbital (fig. 4).

The $I = \frac{5}{2}$ ground state of ^{221}Ra seems to provide evidence for octupole deformation (table 3). It should be mentioned that a modified oscillator single-particle potential gives somewhat different results [35]), however, the radial dependence of the present folded Yukawa potential is expected to give a more reliable extension both to the small ε-values [ref. [2]), p. 214] of the light radium nuclei and to $\varepsilon_3 \neq 0$ [ref. [10]) and subsect. 2.1 above].

The octupole deformation is expected to diminish in ^{229}Ra, but the $[633]\frac{5}{2}$ orbital does not provide a sensitive probe. Hybridization with $[752]\frac{5}{2}$ is maximum at $\varepsilon_3 \sim 0.04$, for still larger ε_3 the magnetic moment goes back toward the value at $\varepsilon_3 = 0$, and the ground state is still $\frac{5}{2}^+$.

The experimental magnetic moment for the $\frac{3}{2}^+$ ground state of $^{227}Ra_{139}$ can only be accounted for by including Coriolis coupling between the reflection asymmetric intrinsic orbitals. The measured moment is $\mu \simeq -0.40$ n.m., which would correspond to an almost pure spin-up orbital under strong coupling. The $\frac{3}{2}$ orbital above the $N = 138$ gap at $\varepsilon_3 = 0.08$ does have a large $\langle \hat{s}_z \rangle$ (fig. 4) due to a large component of $[651]\frac{3}{2}$, and does give a negative μ, but not large enough. In the modified oscillator model [35]), this orbital has a similar behavior as a function of ε_3 but even smaller $\langle \hat{s}_z \rangle$. Coriolis coupling at $\varepsilon_3 = 0$ has little effect [34]), but at $\varepsilon_3 = 0.08$ the $K = \frac{1}{2}$ orbital just below the $N = 138$ gap comes closer in energy, and Coriolis coupling gives a large negative contribution to μ. A $K = \frac{1}{2}$ admixture of slightly less than 2% is sufficient to reproduce the experimental magnetic moment if $g_s/g_s^{\text{free}} = 0.6$, and slightly less than 1% is required if $g_s/g_s^{\text{free}} = 0.7$. Taking the empirical energy separation of the levels, the attenuation factor on the single-particle Coriolis matrix element due to pairing would have to be in the range 0.7–1.0 for this coupling to account for the entire shift of the magnetic moment, which is reasonable. The origin

of the sensitivity in μ is a cross-term of the magnetic operator between the $K=\frac{1}{2}$ and $\frac{3}{2}$ components, where the dominating contribution comes from the large Coriolis matrix element itself ($\langle\frac{3}{2}|\hat{j}_+|\frac{1}{2}\rangle = 5.0$). A similar but weaker effect on μ is also obtained from coupling to the $K=\frac{1}{2}$ orbital at the top of fig. 4. The magnetic moment of the $\frac{3}{2}^+$ ground state in ^{223}Ra can likewise be brought into exact agreement with experiment by a 3% admixture of the $K=\frac{1}{2}$ orbital below the Fermi level. These two strongly interacting orbitals have dominant components $[642]\frac{3}{2}$ and $[651]\frac{1}{2}$, respectively. However, the energy of the $K=\frac{1}{2}$ quasiparticle level is not known experimentally, so it cannot be said whether this amount of mixing is appropriate.

In summary, the experimental data in table 3 can all be accounted for near the equilibrium ε_3 value, but not so well in all cases at $\varepsilon_3 = 0$.

3.4. E1 AND E3 PROPERTIES

Odd multipole deformation entails odd-multipole collective electric moments in the intrinsic frame. The states of good parity after projection into the laboratory frame obviously cannot have such moments, but the odd Eλ moments can nevertheless be measured as transition moments between the members of a parity doublet, just as the intrinsic E2 moment of a 0^+ state can be determined from in-band rotational transitions.

In γ-decay the E1 component dominates, while E3 matrix elements can be obtained from Coulomb excitation using light ions. Results for ^{229}Th and ^{226}Ra are discussed in sect. 4. The only other nucleus which has a sufficiently long half-life for Coulomb excitation by existing techniques is ^{227}Ac. The experiment would be well worthwhile in order to verify the presence of a strong E3 transition between the members of the $K^\pi = \frac{3}{2}^\pm$ doublet, as implied by the M1 data in fig. 10 [also ref. [18])].

The E1 collective dipole moment arises because in the absence of reflection symmetry there is zero probability that the proton center of mass coincides with the neutron center of mass, or the total center of mass about which the nucleus rotates. For intermediate-coupling basis states, the reduced E1 rate within a parity doublet is

$$B(\mathrm{E1};\mathrm{i}\to\mathrm{f}) = |\{(u_\mathrm{i}u_\mathrm{f} - v_\mathrm{i}v_\mathrm{f})\, e_\mathrm{eff}\langle\Psi_\mathrm{i}|rY_{10}|\Psi_\mathrm{f}\rangle + e\hat{Q}_{10}\}\langle I_\mathrm{i}K\,10|I_\mathrm{f}K\rangle|^2 \qquad (K\neq\tfrac{1}{2})\,, \tag{3.5}$$

where the effective charge e_eff in the single-particle term should take into account the center of mass and the giant dipole resonance [eq. (6-330) of ref. [2])]. The collective dipole operator $\hat{Q}_{10}$ is related to the Nilsson shape coordinate ε_1 by eq. (2.15). It is well known that the E1 matrix elements between close-lying Nilsson orbitals are invariably small. Therefore even a small center-of-mass displacement, or condensate of the giant E1 mode into the ground state, has a huge effect on the E1 transition rate within a parity doublet. If the 41 ns lifetime measured in ^{227}Ac can be associated with the $\frac{3}{2}^+$ upper member of the ground-state parity doublet [6]),

the E1 transition within the doublet is about two orders of magnitude faster than the calculated single-particle transition from $[651]\frac{3}{2}$ to $[532]\frac{3}{2}$, even without the pairing *uu-vv* factor on the latter. Assuming that the observed transition has 100% of the collective E1 strength present in the core ground state, the intrinsic electric dipole moment corresponds to $\varepsilon_1 \lesssim 0.0001$, or a displacement of the proton center of gravity by $\lesssim 10^{-3}$ fm.

The lifetimes of excited states are generally not available, but the collectivity of some E1 transitions can be inferred from the branching ratios in γ-decay. One signature is the intensity ratio of E1 branches from an initial state into the different members of a rotational band. Such ratios are governed by the Clebsch–Gordan coefficient in eq. (3.5) in collective cases, as observed [36,37]) for example in ^{227}Ra and ^{229}Th, whereas the tiny single-particle E1 matrix elements are sensitive to changes in rotational perturbations from one band member to the next [2,38]). An absolute measure of the E1 rate is obtained when there is an E1 decay branch in competition with an E2 or M1 transition whose rate can be reliably estimated from other data. For example, the ^{229}Th intermediate coupling calculation in sect. 4 provides moderately accurate values for the mixed M1/E2 rates between the negative-parity levels at 140–240 keV (fig. 13 below). The E1 branches follow eq. (3.5), and from the intensity ratios the collective dipole moment can be inferred to have the same order of magnitude as the value deduced above for ^{227}Ac. In-band B(E2) rates in doubly even nuclei can be more accurately estimated from measured $B(\mathrm{E2}; 2^+ \to 0^+)$ rates. It would be interesting to obtain B(E1) values from the $B(\mathrm{E2}; 3^- \to 1^-)/B(\mathrm{E1}; 3^- \to 2^+)$ branching ratio in doubly even nuclei, to compare with E1 rates in the more closely spaced parity doublets of odd-A neighbors to see if they match. For ^{226}Ra and ^{228}Th, the doubly even neighbors of ^{227}Ac, most of the intensity in the E2 branch would come in the form of very low-energy conversion electrons if the ε_1 value tentatively extracted above for ^{227}Ac is valid.

Recent measurements at high spin in the nuclei ^{218}Ra and ^{222}Th have established a parity-degenerate yrast sequence where E1 cascade transitions compete effectively with the crossover E2 transitions [11,39,40]). This is suggestive of a reflection asymmetric rotor with a relatively large dipole moment corresponding to a shift of the proton center of gravity of the order of 10^{-2} fm. It will be interesting to see in a future investigation whether parity-mixed quasiparticles in the *rotating* intrinsic frame could provide distinctive probes of the structure.

3.5. α-TRANSITIONS

Favored α-transitions occur between similar intrinsic configurations; in doubly even nuclei from the ground state of the parent to the ground state or ground band of the daughter, and in odd-A nuclei from the parent ground state to the band on the same single-particle state in the daughter. The α-transition rates are conveniently

measured by the hindrance factor F, whose inverse F^{-1} is the transition rate in units of the smooth Geiger–Nuttal rate. The latter describes transitions from ground state to ground state in doubly even nuclei quite accurately for almost all nuclei [6]) – a notable exception which confirms the rule is ^{218}Ra [ref. [41])].

If the opposite-parity members of a parity doublet really are just different projections from the same intrinsic state of broken reflection symmetry, then α-transitions to both parities should be allowed. A similar situation has been recognized [2]) for broken symmetry in the intrinsic coordinate frame where particle number plays the role of angular momentum: for example the collective 0^+ excitation at 810 keV in ^{234}U has $F \sim 4$, whereas unfavored transitions typically have $F \sim$ 100–1000. The empirical systematics for α-transitions to the 1^- state in doubly even thorium and radium nuclei is shown by the two upper curves in fig. 11. The hindrance factor goes down markedly at the neutron number where intrinsic reflection asymmetry is expected to set in.

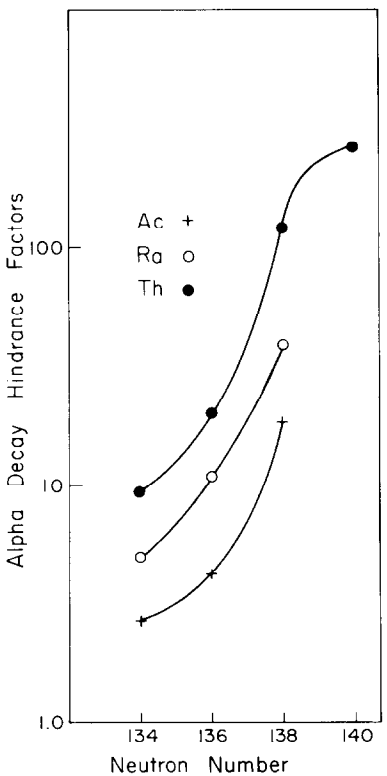

Fig. 11. Experimental hindrance factor [6]) for α-decay to the 1^- state of Th and Ra isotopes, and for parity non-conserving α-decay to the favored doublet in Ac isotopes (fig. 12). For neutron numbers below $N \sim 140$, where instability with respect to octupole deformation is expected to set in, the α-decay changes character from unfavored to favored. This can be interpreted as a change of the 1^- level structure from dynamical vibration to projection out of the intrinsic ground state.

The corresponding α-transition rates are very large compared with transitions to negative-parity states in other doubly even nuclei, and have even given rise to speculations about α-cluster configurations for these states [42]), but they are still small compared to the limit $F = 1$. Some hindrance comes from projection, since decay of 0^+ to 1^- must be p-wave instead of s-wave, but an optical model estimate as in ref.[43]) shows that this is a relatively small part of the observed effect. It would be useful to investigate theoretically which aspects of the deviation from an idealized picture of a static octupole deformation, identical in parent and daughter, might be measured by the excess hindrance.

Given the empirical α-transition rates to octupole bands in doubly even nuclei, they can be used to analyze the data for odd-A nuclei. The available data for favored α-transitions to odd-A parity doublets are shown in fig. 12, where the hindrance factors have been renormalized so that the transition to the analog of the parent ground state has $F = 1$ by definition. Clearly, the parity-changing α-transitions are almost as favored as the natural-parity transitions. The systematics as a function of neutron number are shown by the lower curve in fig. 11, which gives the renormalized hindrance factor to the lowest unnatural-parity state. The curve through the Ac favored doublet data is seen to mimic the curves for doubly even Ra and Th octupole bands.

This result strongly supports an octupole assignment to the proposed parity doublets in ^{223,225,227}Ac. Coupling of the odd-particle motion to reflection asymmetry in the core can then be inferred from the energy splitting between opposite-parity states, which is significantly smaller in the odd-A doublets than the doubly even neighbors. The same argument was forwarded above in the context of decoupling factors (subsect. 3.1).

Further evidence for such coupling is provided by the α-transition rates themselves. The fact that the curve for Ac in fig. 11 lies below the curves for Ra and Th suggests that the intrinsic configurations of opposite-parity states are more similar with the odd proton than without. In order to check that the effect remains when angular momentum is taken properly into account, it is instructive to consider a "weak-coupling" limit where an odd particle of good parity is simply angular-momentum coupled to the empirical doubly even core. The α-transition rate from initial state i to favored final states f in the odd-A nucleus can then be written [2])

$$T(I_i p_i \to I_f p_f) = T_0 \sum_{L_\alpha} F^{-1}(0^+ \to L_\alpha(-)^{L_\alpha}) \langle I_i K L_\alpha 0 | I_f K \rangle^2 , \qquad (3.6)$$

where the core hindrance factors F are taken from experiment for the $K = 0$ ground and octupole bands of the doubly even neighbors, and T_0 is adjusted to experiment for the lowest natural-parity final state in the odd-A daughter. The results obtained with this formula are shown in table 4. The natural-parity states are accurately described, but hindrance factors to the opposite-parity states are grossly overestimated relative to experiment. This suggests that the single-particle state is actually

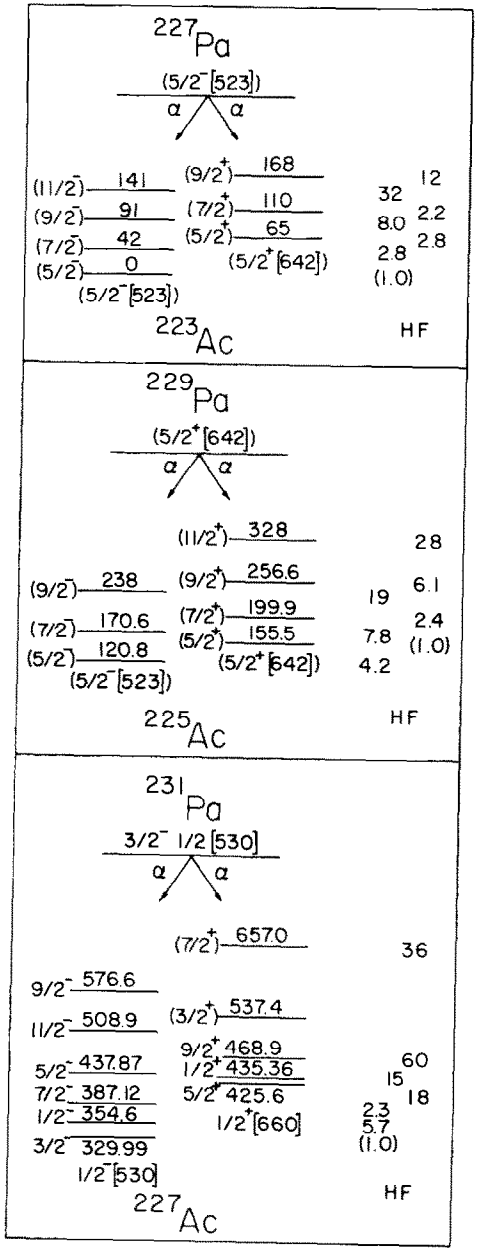

Fig. 12. Experimentally observed favored α-decay into closely spaced parity doublets of odd-A Ac isotopes. The observed hindrance factors to the right of the levels are normalized to unity for the "natural" favored transition. The parity-changing transitions are considerably enhanced relative to the doubly even cores (table 4), suggesting that each of these parity doublets stems from a single parity-mixed Nilsson orbit.

TABLE 4

α-transition rates calculated by eq. (3.6) with empirical core matrix elements from ref. [6])

Final state	L_α	$F^{\text{th}}_{\text{RaTh}}$	$F^{\text{th}}_{\text{Ra}}$	F^{exp}
		$^{223}Ac\ (T_0=0.30)$		
$\frac{5}{2}^-$	0, 2, 4	(2.5)		2.5
$\frac{7}{2}^-$	2, 4, . . .	7.2		7.1
$\frac{9}{2}^-$	2, 4, . . .	18		20
$\frac{5}{2}^+$	1, 3, . . .	31	22	7.0
$\frac{7}{2}^+$	1, 3, . . .		40	5.4
$\frac{9}{2}^+$	3, . . .		120	30
		$^{225}Ac\ (T_0=0.20)$		
$\frac{5}{2}^+$	0, 2, 4	(3.6)		3.6
$\frac{7}{2}^+$	2, 4, 6	9.4		8.8
$\frac{9}{2}^+$	2, 4, 6	24		22
$\frac{5}{2}^-$	1, 3, 5	110	74	15
$\frac{7}{2}^-$	1, 3, 5	230	240	28
$\frac{9}{2}^-$	3, 5, . . .	1250	520	68
		$^{227}Ac\ (T_0=0.36)$		
$\frac{3}{2}^-$	0, 2	(2.3)		2.3
$\frac{1}{2}^-$	2	14		13
$\frac{7}{2}^-$	2, 4	5.3		5.2
$\frac{5}{2}^+$	1, 3	370	180	42
$\frac{7}{2}^+$	3, 5	6400	9100	83
$\frac{9}{2}^+$	3, 5	13 000	2100	140

For each final nucleus, the value of T_0 is chosen to fit one level and is indicated in units of the Geiger–Nuttal value. The first column indicates the final state (fig. 12). The second column lists the L_α values included in the summation, dots indicate values missing because empirical data for the core are unavailable. The third column shows calculated hindrance factors using the neighboring radium core. The fourth column shows calculated hindrance factors with core values averaged between the neighboring radium and thorium cores – there is a significant difference for odd L_α. The fifth column shows experimental hindrance factors without the renormalization used in figs. 11 and 12. Note that the calculated hindrance factors for parity-changing transitions are much too large, which suggests that the odd particle is actually in a parity-mixed Nilsson orbital.

parity-mixed. In that case the change in parity can be achieved within the single-particle state, and the transition strength in the parity-conserving core matrix elements, which are by far the largest, can also contribute to transitions which change the parity of the core-particle system.

3.6. ODD-ODD NUCLEI

Little spectroscopy has been done so far on doubly odd nuclei in the $A \sim 220$–230 region, and there are almost no spin-parity assignments. A general remark can be made on the basis of the present model, which is straightforwardly generalized to the odd-odd case. The part of the hamiltonian which determines the parity splitting of strong-coupled states becomes

$$-\tfrac{1}{2}E\hat{P} = -\tfrac{1}{2}Ep\hat{\pi}_{\mathrm{p}}\hat{\pi}_{\mathrm{n}}\,; \tag{3.7}$$

in other words, the parity-splitting which is E in the doubly even case is reduced by a factor $\langle\hat{\pi}_{\mathrm{p}}\rangle$ for the odd proton and a factor $\langle\hat{\pi}_{\mathrm{n}}\rangle$ for the odd neutron. In odd-A nuclei, each of these factors is found empirically to be about $\frac{1}{2}$ to $\frac{1}{100}$ and thus the average energy splitting of parity doublets in doubly odd nuclei should be significantly smaller [cf. the comparison of doubly even and singly odd nuclei in ref. [10])]. In particular, there is a good probability of finding some parity doublets so nearly degenerate that it would be possible to study the parity mixing in the laboratory frame caused by the weak interaction [e.g. ref. [44]) and references therein, and ref. [12])].

4. Octupole vibration-deformation transition at $A \sim 229$

The theoretical potential-energy curves in fig. 6 indicate that a transition takes place in the francium-uranium region between octupole deformation for nuclei with mass number $A < 229$ and octupole vibration for heavier nuclei. Experimental investigations of E1 and E3 properties in the ^{229}Th nucleus have recently demonstrated that one Nilsson orbital supports octupole vibrations, while another seems rather to be octupole deformed [37,45]). In this section a calculation is described which accounts for the data and shows that they are consistent with the potential-energy curve of fig. 6 and the underlying single-particle scheme.

4.1. DETAILS OF THE CALCULATION

In order to take into account the soft anharmonic structure of the ^{229}Th core the calculation is carried out in the intermediate-coupling scheme. The core is described by the hamiltonian of one-dimensional collective motion in the potential of fig. 6, parametrized as

$$V(\varepsilon_3) = \tfrac{1}{2}C\varepsilon_3^2 + D(\mathrm{e}^{-\varepsilon_3^2/a^2} - 1)\,.$$

The parameters C, D and a are determined by averaging between the neighboring cores. Here $C = 156$ MeV while D and a are related to the average depth (0.16 MeV) and position ($\bar{\varepsilon}_3 = 0.046$) of the minimum. The inertial mass is set equal

to a constant, $B = 330.7\,\hbar^2 \cdot \mathrm{MeV}^{-1}$, chosen to reproduce the experimental energy (512 keV) of the $\frac{5}{2}^-$ octupole vibration on the $\frac{5}{2}^+$ ground state of ^{229}Th. This puts the core $K^\pi = 0^-$ level near the excitation energy observed experimentally in ^{230}Th, significantly higher than the energy observed in ^{228}Th. Such an *ad hoc* choice is often required in core-particle coupling when the odd-A nucleus is sandwiched into a phase transition between two very different even neighbors. A generalization of intermediate coupling has been proposed [46]) which might be able to deal with sharp quadrupole phase transitions by taking both cores into account, and in the future it may be worthwhile to study a corresponding formalism for the $A \sim 229$ octupole phase transition. Another shortcoming of the present model is reflected in the collective E3 transition rate. The calculated $B(\mathrm{E3}; 3^- \to 0^+)$ value for the core is 17 s.p.u., 0.56 times the measured value [47]) 29 s.p.u. in ^{230}Th. The missing strength can be attributed to the $K \neq 0$ octupole modes which couple coherently to the 3^- level by the Coriolis interaction. Thus, for example, in the calculation by Neergård and Vogel [5]) for ^{230}Th the contribution from the $K = 0$ mode is 0.64 times the total calculated $B(\mathrm{E3})$ value. The effect of coupling to the $K \neq 0$ octupole modes is expected to decrease for $A < 229$ since the $K = 0$ mode comes down in energy, and the measured [48]) $B(\mathrm{E3})$ value for ^{226}Ra is in fact fully accounted for by the calculated $K = 0$ octupole deformation [10]).

The six lowest solutions of the $K = 0$ collective octupole hamiltonian constitute the core space of the intermediate-coupling calculation. The core rotational moment of inertia parameter is set to $\hbar^2/2\mathcal{I} = 0.009$ MeV for the $K^\pi = 0^+$ ground-state rotational band and 0.0065 MeV for rotational bands on the other core states, which is close to the empirical value for both ^{228}Th and ^{230}Th.

The single-particle orbitals and the BCS transformation is computed in the folded Yukawa single-particle model at an average point between the reflection symmetric constrained equilibrium deformations for ^{228}Th and ^{230}Th: $\varepsilon_2 = 0.17$, $\varepsilon_4 = -0.08$ and $\varepsilon_6 = 0.017$. Sixteen single-neutron levels, 8 above and 8 below the Fermi level, are included in the coupling calculation. The adiabatic part of the intermediate coupling hamiltonian was solved and compared with the folded Yukawa levels as a function of ε_3. The rescaling of the abscissa which gives the best agreement is obtained for the intermediate-coupling constant $k = 0.8$. Four low-lying Nilsson levels have been established in experiments [37]) on ^{229}Th, and to get their relative energies exactly right in the intermediate coupling calculation it is necessary to make some empirical adjustments. The following increments were added to the theoretical quasiparticle energies: $[633]\frac{5}{2}$, -145 keV; $[631]\frac{3}{2}$, 0; $[752]\frac{5}{2}$, 118 keV; $[761]\frac{3}{2}$, 478 keV. These numbers are somewhat larger than the expected inaccuracy of the folded Yukawa scheme because they also include the effect of the particle-rotor recoil term, which is not included explicitly. The empirical Coriolis coupling strength between the $j_{15/2}$ levels has previously been analyzed [37]), and similar results are obtained in the present work by the usual *ad hoc* prescription [49]) of raising all pairing $u_iu_j + v_iv_j$ factors to power 3.

4.2. RESULTS FOR ^{229}Th

The main experimental features of the ^{229}Th spectrum are shown to the right in fig. 13. The low-lying levels of both positive and negative parity can be grouped into two sets with $K=\frac{3}{2}$ and $K=\frac{5}{2}$, respectively. The $\Delta K=0$ parity-changing collective excitation appears at low energy (164 keV) when it is based on the lowest $K=\frac{3}{2}$ level, but higher in energy (512 keV) when based on the lowest $K=\frac{5}{2}$ level. This will be interpreted as octupole shape coexistence depending on the single-particle configuration in the transitional nucleus. The intermediate-coupling model is able

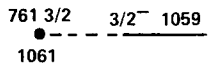

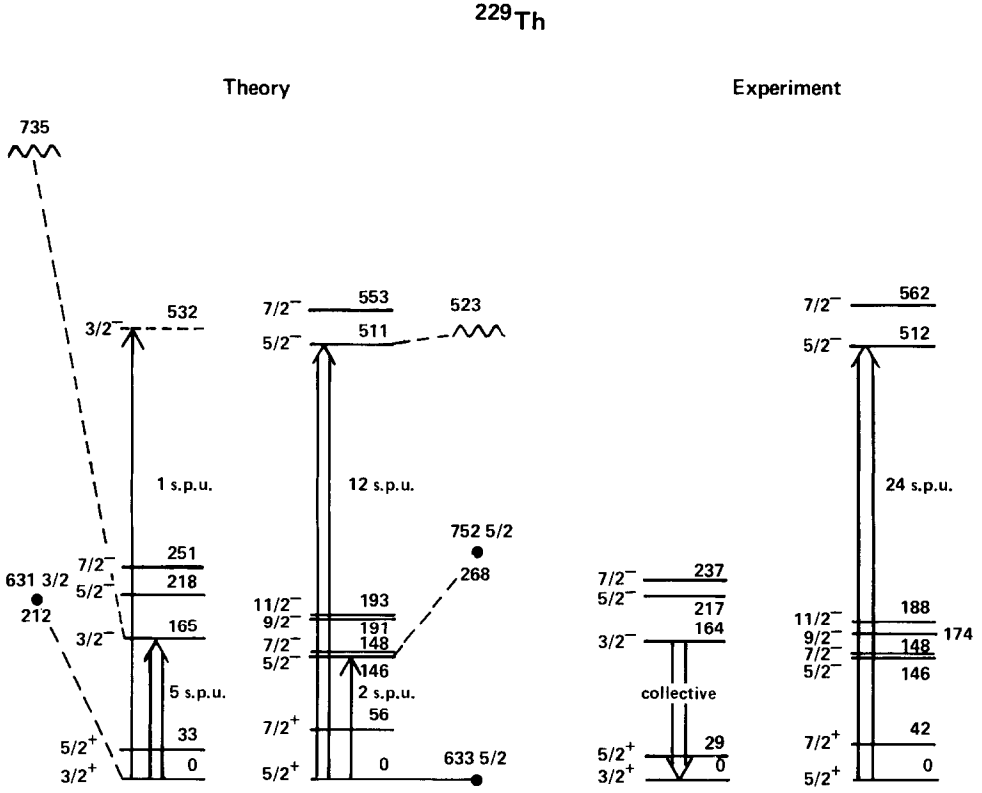

Fig. 13. Partial level scheme for ^{229}Th from an intermediate-coupling calculation with a soft core and from experiment. The different character of the octupole mode for $K=\frac{3}{2}$ (left) and $K=\frac{5}{2}$ (right in each spectrum) can be understood on the basis of the analytical model in subsect. 2.4. For $K=\frac{3}{2}$ the second unperturbed Nilsson orbital (black dot) comes above the unperturbed octupole vibration on the lowest orbital and pushes the octupole down, but for $K=\frac{5}{2}$ it comes below. In the full calculation, core polarization enhances the effect for $K=\frac{3}{2}$.

to reproduce the data as shown in the left part of fig. 13, and it is interesting to see how and why.

First let us briefly review how the experimental features in fig. 13 were extracted from the measurements. The E3 matrix elements from the $\frac{5}{2}^+$ ground state of ^{229}Th were measured directly by Coulomb excitation with α-particles [45]). The discrepancy in fig. 13 between the theoretical and experimental $B(\mathrm{E3}; \frac{5}{2}^+ \rightarrow \frac{5}{2}^-)$ value probably reflects the discrepancy in the core which was discussed in the previous subsection and attributed to the neglect of $K > 0$ octupole modes. The $\frac{3}{2}^+$ level very near the ground state and the associated low-lying collective strength was inferred [37]) from γ-ray studies following the α-decay of ^{233}U. The negative-parity levels from 146 to 237 keV were interpreted in terms of Coriolis coupling within the $j_{15/2}$ shell. It was noticed that the E1 transitions from these levels do not populate the $K^\pi = \frac{5}{2}^+$ rotational band but another positive-parity band, and that the E1 branching ratios into the latter band closely follow Clebsch–Gordan coefficients with $K = \frac{3}{2}$ (cf. eq. (3.5)).

The essential Nilsson levels and off-diagonal couplings of the intermediate coupling theory, arranged in correspondence with fig. 13, are as follows:

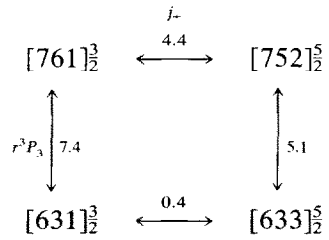

The theoretical octupole matrix elements, given for r^3P_3 in dimensionless stretched oscillator units, are about equal for $K = \frac{3}{2}$ and $\frac{5}{2}$. The $[631]^3_2$ and $[633]^5_2$ assignments are confirmed experimentally by the M1 moments extracted from measured mixing ratios [37]). The Coriolis coupling between these two low-lying levels is weak, while Coriolis coupling to higher-lying positive-parity levels is more important for $[631]^3_2$ than $[633]^5_2$ as evidenced by the rotational moment of inertia and, in the calculation, the lowering of the band-head energy. The position of the unperturbed Nilsson quasiparticle levels is indicated by black dots in fig. 13.

The two wavy lines in fig. 13 show the position of the core octupole excitation based on the unperturbed $K^\pi = \frac{3}{2}^+$ and $\frac{5}{2}^+$ levels, respectively. For $K = \frac{3}{2}$ the wavy line comes between the black dots, for $K = \frac{5}{2}$ it lies above them. From this fact alone, the different octupole energies for $K = \frac{3}{2}$ and $\frac{5}{2}$ can be understood qualitatively using the analytical model described in subsect. 2.4.

However, it should be emphasized that "multiphonon" octupole excitations of the core which are included in the present calculation play a major role for the quantitative agreement between theory and experiment in fig. 13. The low-lying octupole excitation at 165 keV for $K = \frac{3}{2}$ would go up to 362 keV if core excitations

TABLE 5

Wave functions obtained from the intermediate-coupling calculation for ^{229}Th

$|\frac{5}{2}^+\rangle_0 = 0.985|633\frac{5}{2}^+; 0\rangle + 0.119|752\frac{5}{2}^+; 1\rangle + \cdots$
$|\frac{5}{2}^-\rangle_{146} = 0.750|752\frac{5}{2}^-; 0\rangle + K = \frac{3}{2}$ Coriolis admixtures $+ \cdots$
$|\frac{5}{2}^-\rangle_{511} = 0.953|633\frac{5}{2}^-; 1\rangle + \cdots$
$|\frac{3}{2}^+\rangle_0 = 0.876|631\frac{3}{2}^+; 0\rangle - 0.364|761\frac{3}{2}^+; 1\rangle - 0.210|631\frac{3}{2}^+; 2\rangle + \cdots$
$|\frac{3}{2}^-\rangle_{165} = 0.743|631\frac{3}{2}^-; 1\rangle - 0.463|761\frac{3}{2}^-; 0\rangle + 0.306|761\frac{3}{2}^-; 2\rangle + \cdots$
$|\frac{3}{2}^-\rangle_{532} = 0.720|750\frac{1}{2}^-; 0\rangle + 0.510|651\frac{1}{2}^-; 1\rangle - 0.350|750\frac{1}{2}^-; 2\rangle + \cdots$

The basis states are given as $|Nn_z\Lambda\Omega; n_3\rangle$ where the single-particle quantum numbers correspond to the labelling in fig. 2, and n_3 is a counting number for the $K = 0$ anharmonic octupole excitations of the core.

above the first anharmonic octupole excited state were taken out of the basis. Table 5 gives the theoretical wave functions in the intermediate coupling basis. The $\frac{5}{2}^+$ ground state is a clean reflection-symmetric Nilsson level, and the $\frac{5}{2}^-$ state at 511 keV is obtained by the excitation of one anharmonic octupole "phonon" in the core. The intrinsic parities are more strongly mixed in the $\frac{3}{2}^\pm$ parity doublet at 0 and 165 keV, and there are significant components of core states with $n_3 > 1$ which represent polarization to larger ε_3 deformations. (Theory also gives a strongly polarized and parity-mixed $K = \frac{1}{2}$ band at ~500 keV.) The single-particle parity mixing and the core octupole deformation of the wave functions in table 5 are indicated by the matrix elements in table 6. The two states of a parity doublet would have identical matrix elements in the extreme limit of strong coupling to octupole deformation. Clearly the $K = \frac{3}{2}$ doublet at 0 and 165 keV is closer to this limit than the $K = \frac{5}{2}$ doublet at 0 and 511 keV, with regard to $\langle\varepsilon_3^2\rangle^{1/2}$.

TABLE 6

The expectation value of the single-particle parity, $\langle\pi\rangle$, and rms octupole deformation of the core, $\langle\varepsilon_3^2\rangle^{1/2}$, obtained theoretically for some states in ^{229}Th

	$\langle\pi\rangle$	$\langle\varepsilon_3^2\rangle^{1/2}$
$\|\frac{5}{2}^+\rangle_0$	+0.98	0.054
$\|\frac{5}{2}^-\rangle_{146}$	−0.45	0.076
$\|\frac{5}{2}^-\rangle_{511}$	+0.83	0.083
$\|\frac{3}{2}^+\rangle_0$	+0.67	0.064
$\|\frac{3}{2}^-\rangle_{165}$	+0.27	0.083
$\|\frac{3}{2}^-\rangle_{532}$	−0.35	0.075
$\|0^+\rangle_0$	0	0.053
$\|0^-\rangle_{523}$	0	0.084

The deviation of $\langle\pi\rangle$ from +1 or −1 indicates the single-particle parity mixing. Naked core values for $\langle\varepsilon_3^2\rangle^{1/2}$ are given for comparison at the bottom of the table.

5. Summary and conclusions

The unified model of Bohr, Mottelson and Nilsson [1,2,14]) deals with spontaneous symmetry-breaking of the nuclear mean field in the intrinsic frame and describes its relation to the motion of individual nucleons. The present paper gives a specific formulation, useful for studying the parity-breaking reflection asymmetric mode of symmetry $C_{\infty h}$. This kind of symmetry breaking is known to occur in nuclei of the radium region, the main question has been whether it is a static ground-state property or a dynamical excitation mode. [It might also occur for example in neutron-rich isotopes of Ba-La and Kr-Rb produced by the fission of heavy actinides [10]).]

The odd particle is used as a probe of the intrinsic mean field. In sect. 3 the criterion for a "static" reflection asymmetric deformation is taken to be a significant improvement over a reflection symmetric description of spectroscopic data, just as the original Nilsson scheme was an improvement over the spherical shell model. It may be required that:

(i) the symmetry breaking is a consequence of the model, so that the amount of deformation is determined self-consistently in each case, and

(ii) instead of accounting for *some* spectroscopic data in *most* cases, the model should account for *most* of the pertinent data in *all* cases.

The initial choice of single-particle potential is important if a detailed comparison with experiment is to be made. The investigation above and in ref. [10]) has shown that the folded Yukawa model in a form fixed by the Los Alamos–Lund collaboration [8,19,20]) appears to work well with respect to both of the above requirements. It should be emphasized that the calculated results in sects. 2 and 3 are unambiguous results of a self-contained theory whose parameters were fixed prior to the start of the investigation.

The quasiparticle band-head energies are mostly described on the same level of accuracy as in the heavier actinides where the parameters were once fitted, using either the reflection asymmetric equilibrium shape for $A < 229$ or the constrained equilibrium at $\varepsilon_3 = 0$, but there are some notable exceptions. For example, both experiment and the theory with reflection asymmetry give a $K^\pi = \frac{1}{2}^\mp$ ground-state doublet in ^{225}Ra, which cannot be accounted for at $\varepsilon_3 = 0$.

Several other parity doublets, closely spaced in energy, are known experimentally in odd-A Ra, Ac, Th and Pa isotopes. Such doublets might originate from a single parity-mixed Nilsson orbital in an adiabatically octupole-deformed mean field (strong coupling), or alternatively from two distinct single-particle orbitals in a reflection symmetric field which are only partly mixed by the collective octupole excitation mode in the core (weak or intermediate coupling). Several items of experimental information were used in sect. 3 to distinguish between the two alternatives. If there is a parity-mixed Nilsson orbital, the magnetic g-factor should be the same for both members of the doublet. Likewise, for $K = \frac{1}{2}$ the decoupling factor times the parity, referred to as the decoupling "invariant", should be the

same. The electric dipole and octupole transition rates between the two members should have the full collective strength from the core. Favored α-decay should populate both members of the final-state parity doublet about equally. In conjunction with any of the above, a reduction of the odd-A parity splitting relative to the core becomes indicative.

Relative to the experimental data on all these aspects, strong coupling does in fact give a uniform improvement over weak coupling. All the ground-state spins and magnetic moments in the radiums [34]) can be accounted for. The measured magnetic g-factors in the $\frac{3}{2}^{\pm}$ ground-state doublet of ^{227}Ac indicate that the strong-coupling limit is realized in this case [31]). Anomalous decoupling invariants in ^{225,227}Ra [refs. [30,36])] are explained. There are parity-changing α-transitions almost as favored as the favored parity-conserving transitions, and a quantitative phenomenological analysis of odd-A relative to even-A α-decay data indicates the need for intrinsic parity mixing.

However, although there is an approach toward the strong-coupling limit in most cases, it seems to be reached only in a few cases. For example, decoupling invariants approach each other but do not become identical. This does not contradict the presence of a static octupole deformation: just as decoupling from the rotational asymmetry is induced by the Coriolis matrix elements and had to be included above to account for the magnetic moments of ^{223,227}Ra, so there can also be decoupling from the reflection asymmetry. The analog of the single-particle Coriolis matrix element of $\hat{j}_+$ is the off-diagonal matrix element of the single-particle parity operator $\hat{\pi}$. Such parity decoupling is demonstrated using the analytical model of subsect. 2.4. Taking off-diagonal matrix elements into account, identical results are obtained in the strong- and weak-coupling representations, except for a certain effect due to pairing.

Nevertheless, core softness is expected to play a role in some of the situations intermediate between strong and weak coupling. The coexistence of strong- and weak-coupled states in the octupole transitional nucleus ^{229}Th is well described in the present work using a weak coupling basis and the soft calculated potential. The wave functions in the more strongly coupled doublet then turn out to include a condensate of high-lying core octupole excitations, corresponding to core polarization.

In summary, the unified model based on a single-particle potential of folded Yukawa type, which implies rather stable reflection asymmetric intrinsic ground states in the Fr-Pa region, gives agreement in considerable detail with the available experimental data on odd-A nuclei in this region. Accepting the presence of such asymmetry opens up interesting areas to explore in the future, for example the phase transition at $A \sim 229$ which to a fair approximation has the remarkable property of being one-dimensional, deviations from the strong-coupling limit for $A < 229$, reflection asymmetry at high spins, and perhaps in odd-odd nuclei parity non-conservation in the laboratory frame.

Discussions with many colleagues doing related work have been stimulating and helpful. Special acknowledgement is due to Y.A. Ellis-Akovali for contributions to the analysis of α-transition data, to I. Hamamoto for clarifying comments on step (v) of the strong coupling scheme, to R. Neugart for communicating laser measurement data prior to publication and to A.J. Sierk at the Los Alamos end of the calculations. This work was supported in part by the National Science Foundation under contract PHY-79-08395, the Swedish Natural Science Research Council and the US Department of Energy under contract no. DE-AC05-760R00033 with Oak Ridge Associated Universities.

References

1) A. Bohr, Mat. Fys. Medd. Dan. Vid. Selsk. **26**, No. 14 (1952)
2) A. Bohr and B.R. Mottelson, Nuclear structure, vol. 2 (Benjamin, New York, 1975)
3) K. Alder, A. Bohr, T. Huus, B. Mottelson and A. Winther, Rev. Mod. Phys. **28** (1956) 432
4) F. Stephens, F. Asaro and I. Perlman, Phys. Rev. **96** (1954) 1568; **100** (1955) 1543
5) K. Neergård and P. Vogel, Nucl. Phys. **A145** (1970) 33; **A149** (1970) 209, 217
6) Table of isotopes, ed. C.M. Lederer and V.S. Shirley (Wiley, New York, 1976)
7) W. Kurcewicz, E. Ruchowska, N. Kaffrell, T. Björnstad and G. Nyman, Nucl. Phys. **A356** (1981) 15
8) P. Möller and J.R. Nix, Nucl. Phys. **A361** (1981) 117
9) A. Gyurkovich, A. Sobiczewski, B. Nerlo-Pomorska and K. Pomorski, Phys. Lett. **105B** (1981) 95
10) G.A. Leander, R.K. Sheline, P. Möller, P Olanders, I. Ragnarsson and A.J. Sierk, Nucl. Phys. **A388** (1982) 452
11) J. Fernandez-Niello, H. Puchta, F. Riess and W. Trautmann, Nucl. Phys. **A391** (1982) 221
12) I. Ahmad, J.E. Gindler, R.R. Betts, R.R. Chasman and A.M. Friedman, Phys. Rev. Lett. **49** (1982) 1758
13) M. Gai, J.F. Ennis, M. Ruscev, E.C. Schloemer, B. Shivakumar, S.M. Sterbenz, N. Tsoupas and D.A. Bromley, Phys. Rev. Lett. **51** (1983) 646
14) S.G. Nilsson, Mat. Fys. Medd. Dan. Vid. Selsk. **29**, No. 16 (1955)
15) H.J. Krappe and U. Wille, Nucl. Phys. **A124** (1969) 641
16) A. Faessler, Y. Udagawa and R.K. Sheline, Nucl. Phys. **85** (1966) 670
17) R.R. Chasman, Phys. Rev. Lett. **42** (1979) 630
18) R.R. Chasman, Phys. Lett. **96B** (1980) 7
19) M. Bolsterli, E.O. Fiset, J.R. Nix and J.L. Norton, Phys. Rev. **C5** (1972) 1050
20) P. Möller, S.G. Nilsson and J.R. Nix, Nucl. Phys. **A229** (1974) 292
21) B.R. Mottelson and S.G. Nilsson, Mat. Fys. Skr. Dan. Vid. Selsk. **1**, No. 8 (1959)
22) R.R. Chasman, I. Ahmad, A.M. Friedman and J.R. Erskine, Rev. Mod. Phys. **49** (1977) 833
23) J.P. Boisson and R. Piepenbring, Nucl. Phys. **A168** (1971) 385
24) E. Osnes, J. Rekstad and O.K. Gjøtterud, Nucl. Phys. **A253** (1975) 45
25) K. Schreckenbach, A.I. Namenson, W.F. Davidson, T. von Egidy, H.G. Börner, J.A. Pinston, R.K. Smither, D.D. Warner, R.F. Casten, M.L. Stelts, D.H. White and W. Stöffl, Nucl. Phys. **A376** (1982) 149
26) R. Zimmermann, Phys. Lett. **113B** (1982) 199
27) S.G. Rohozinski and W. Greiner, Phys Lett. **128B** (1983) 1
28) S.G. Rohozinski, M. Gajda and W. Greiner, J. of Phys. **G8** (1982) 787
29) J. Meyer-ter-Vehn, Nucl. Phys. **A249** (1975) 111
30) K. Nybø, T.F. Thorsteinsen, G. Løvhøiden, E.R. Flynn, J.A. Cizewski, R.K. Sheline, D. Decman, D.K. Burke, G. Sletten, P. Hill, N. Kaffrell, W. Kurcewicz and G. Nyman, Nucl. Phys. **A**, submitted
31) R.K. Sheline and G. A. Leander, Phys. Rev. Lett. **51** (1983) 359
32) W. Teoh, R.D. Connor and R. H. Betts, Nucl. Phys. **A319** (1979) 122
33) I. Anicin, I. Bikit, C. Girit, H. Güven, W.D. Hamilton and A.A. Yousif, J. of Phys. **G8** (1982) 369

34) S. A. Ahmad, W. Klempt, R. Neugart, E. W.Otten, K. Wendt and C. Ekström, Phys. Lett. **B**, submitted
35) I. Ragnarsson, Phys. Lett **B**, in press
36) T. von ! gidy, G. Barreau, H.G. Börner, W.F. Davidson, J. Larysz, D.D. Warner, P.H.M. van Assche, K. Nybø, T.F. Thorsteinsen, G. Løvhøiden, E.R. Flynn, J.A. Cizewski, R.K. Sheline, D. Decman, D.G. Burke, G. Sletten, N. Kaffrell, W. Kurcewicz, T. Björnstad and G. Nyman, Nucl. Phys. **A365** (1981) 26
37) L.A. Kroger and C.W. Reich, Nucl. Phys. **A259** (1976) 29
38) F.M. Bernthal and J.O. Rasmussen, Nucl. Phys. **A101** (1967) 513
39) D. Ward, G.D. Dracoulis, J.R. Leigh, R.J. Charity, D.J. Hinde and J.O. Newton, Nucl. Phys. **A406** (1983) 591
40) W. Bonin, M. Dahlinger, S. Glienke, E. Kankeleit, M. Krämer, D. Habs, B. Schwartz and H. Backe, Z. Phys. **A310** (1983) 249
41) E. Roeckl, Nucl. Phys. **A400** (1983) 131c
42) F. Iachello and A.D. Jackson, Phys. Lett. **108B** (1982) 151
43) J.O. Rasmussen, Phys. Rev. **113** (1959) 1593
44) K. Elsener, W. Grüebler, V. König, C. Schweizer, P.A. Schmelzbach, J. Ulbricht, F. Sperisen and M. Merdzan, Phys. Lett. **117B** (1982) 167
45) C.E. Bemis, F.K. McGowan, J.L.C. Ford, W.T. Milner, R.L. Robinson, P.H. Stelson and C.W. Reich, to be published
46) F. Dönau and S. Frauendorf, Phys. Lett. **71B** (1977) 263
47) F.K. McGowan, C.E. Bemis, W.T. Milner, J.L.C. Ford, R.L. Robinson and P.H. Stelson, Phys. Rev. **C10** (1974) 1146
48) R. Zimmermann, thesis, Munich (1980)
49) F.S. Stephens, P. Kleinheinz, R.K. Sheline and R.S. Simon, Nucl. Phys. **A222** (1974) 235